

Multi-Output Conformal Regression: A Unified Comparative Study with New Conformity Scores

Victor Dheur¹Naomi Desobry¹¹University of MonsMatteo Fontana²²Royal Holloway, University of LondonYorick Estievenart¹Souhaib Ben Taieb^{1,3}³Mohamed bin Zayed University of Artificial Intelligence

Abstract

Quantifying uncertainty in multivariate regression is essential in many real-world applications, yet existing methods for constructing prediction regions often face limitations such as the inability to capture complex dependencies, lack of coverage guarantees, or high computational cost. Conformal prediction provides a robust framework for producing distribution-free prediction regions with finite-sample coverage guarantees. In this work, we present a unified comparative study of multi-output conformal methods, exploring their properties and interconnections. Based on our findings, we introduce two classes of conformity scores that achieve asymptotic conditional coverage: one is compatible with any generative model, and the other offers low computational cost by leveraging invertible generative models. Finally, we conduct a comprehensive empirical study across 32 tabular datasets to compare all the multi-output conformal methods considered in this work. All methods are implemented within a unified code base¹ to ensure a fair and consistent comparison.

1 INTRODUCTION

Quantifying uncertainty in model predictions is crucial in many real-world applications, often involving prediction problems with multiple output variables and complex statistical dependencies. For example, in medical diagnostics, the progression of a disease can be studied by analysing multiple health indicators that exhibit nonlinear dependencies, such as blood pressure

¹<https://github.com/Vekteur/multi-output-conformal-regression>

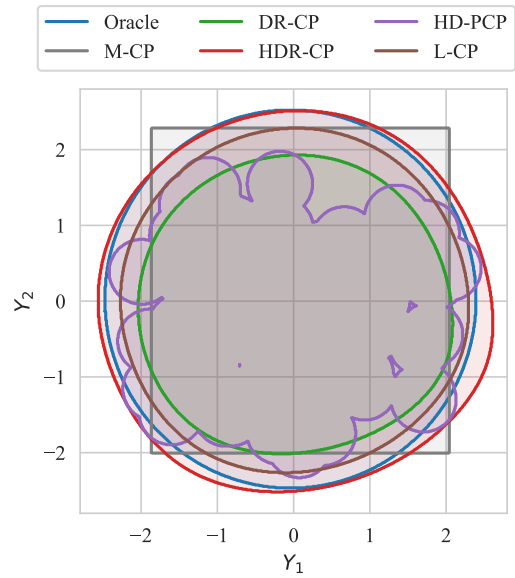


Figure 1: Examples of conditional bivariate prediction regions with 80% marginal coverage for a toy example.

and cholesterol levels of a patient (Rajkomar et al., 2018). Although modern probabilistic and generative AI models can model complex relationships between variables, they can produce unreliable or overly confident predictions (Nalisnick et al., 2018). Figure 1 illustrates bivariate prediction regions for the different conformal methods considered in this paper.

Conformal prediction (CP) offers a robust framework for improving model reliability by generating distribution-free prediction regions with a finite-sample coverage guarantee (Vovk et al., 1999). Although substantial research has focused on univariate prediction problems (Romano et al., 2019; Sesia and Romano, 2021; Rossellini et al., 2023), multivariate settings have received less attention. Among existing work, Zhou et al. (2024b) achieves marginal coverage by combining univariate prediction regions, but fails to capture dependencies between variables. Other methods, such

as density-based approaches (Izbicki et al., 2022) or sample-based techniques (Wang et al., 2023b; Plassier et al., 2024), suffer from high computational costs. An alternative method (Sadinle et al., 2016) optimises the size of the region, but does not achieve asymptotic conditional coverage.

Our *first contribution* is to provide a survey and analysis of conformal prediction methods for multivariate regression within a unified framework, highlighting their similarities, differences, and various properties, while also exploring the connections between them.

Our *second contribution* is the introduction of two new classes of conformity scores: CDF-based and latent-based. The CDF-based scores leverage the CDF of any conformity score and achieve asymptotic conditional coverage. We also propose a specific instance that builds on PCP from Wang et al., 2023b and HPD-split from Izbicki et al., 2020, which has the advantage of not requiring the estimation of a predictive density, relying solely on samples from any generative model. The latent-based scores are inspired by Feldman et al., 2023 and can be interpreted as an extension of distributional conformal prediction (Chernozhukov et al., 2021) for multivariate outputs. Compared to Feldman et al., 2023, our approach does not require directional quantile regression, and the conformalization is performed directly in the latent space, eliminating the need to construct a grid. This enhances both computational efficiency and scalability.

Finally, as our *third contribution*, we conduct a large-scale empirical study comparing the different multi-output conformal methods across 32 tabular datasets with multivariate outputs, evaluating several performance metrics. We consider a variety of multivariate regression models, namely Multivariate Quantile Function Forecaster (Kan et al., 2022), Distributional Random Forests (Cevic et al., 2022), and a multivariate Gaussian Mixture Model parameterized by a hypernetwork (Ha et al., 2022; Bishop, 1994).

2 BACKGROUND

Consider a multivariate regression problem where the objective is to predict a d -dimensional response vector $y \in \mathcal{Y} = \mathbb{R}^d$ based on a feature vector $x \in \mathcal{X} \subseteq \mathbb{R}^p$. We assume there exists a true joint distribution F_{XY} over $\mathcal{X} \times \mathcal{Y}$, and we have access to a dataset $\mathcal{D} = \{(X^{(j)}, Y^{(j)})\}_{j=1}^n$ where $(X^{(j)}, Y^{(j)}) \stackrel{\text{i.i.d.}}{\sim} F_{XY}$. Given a feature vector x , we denote the conditional distribution of Y given $X = x$ as $F_{Y|x}$, and the associated probability density function (PDF) as $f_{Y|x}$.

Based on any base predictor $\hat{h} : \mathcal{X} \rightarrow \mathcal{S}$ (e.g., neural network, decision tree) that maps the input to a space

\mathcal{S} , several methods can be used to define a prediction region for the output. The nature of \mathcal{S} depends on the output of the predictor. If \hat{h} estimates the conditional mean, then $\mathcal{S} = \mathcal{Y}$. If \hat{h} is a density estimator, then $\mathcal{S} = \mathcal{F}(\mathcal{Y})$, where $\mathcal{F}(\mathcal{Y})$ denotes the space of probability density functions (PDFs) over \mathcal{Y} .

A prediction region consists of a set of values that are likely to occur with a pre-specified probability. However, if the model is misspecified or lacks sufficient training data, it may poorly approximate the true conditional distribution. As a result, prediction regions based solely on the model’s estimates may be unreliable and fail to capture the actual underlying uncertainty.

Using the dataset \mathcal{D} , for any $x \in \mathcal{X}$, CP allows us to transform base predictors \hat{h} into calibrated, distribution-free prediction regions $\hat{R}(x) \subseteq \mathcal{Y}$ for the true output y with finite-sample coverage guarantees.

2.1 Split-conformal prediction

Split-conformal prediction (SCP, Papadopoulos et al., 2002) is a computationally efficient variant of conformal prediction that divides the dataset \mathcal{D} into two disjoint subsets: a training set $\mathcal{D}_{\text{train}}$ and a calibration set \mathcal{D}_{cal} . A model is first trained on $\mathcal{D}_{\text{train}}$ to obtain a base predictor \hat{h} . Based on \hat{h} , a conformity score function $s : \mathcal{X} \times \mathcal{Y} \rightarrow \mathbb{R}$ is defined, where lower scores indicate a better fit between the feature vector x and the response y . The calibration scores $\{s_i\}_{i=1}^{|\mathcal{D}_{\text{cal}}|} := \{s(x, y) : (x, y) \in \mathcal{D}_{\text{cal}}\}$ are then computed, from which the $(1 - \alpha)$ empirical quantile is calculated as:

$$\hat{q} = \text{Quantile} \left(\{s_i\}_{i=1}^{|\mathcal{D}_{\text{cal}}|} \cup \{\infty\}; \frac{k_\alpha}{|\mathcal{D}_{\text{cal}}| + 1} \right), \quad (1)$$

where $k_\alpha = \lceil (|\mathcal{D}_{\text{cal}}| + 1)(1 - \alpha) \rceil$. This quantile serves as the threshold for constructing prediction regions. For a new input x , the (random) prediction region is given by:

$$\hat{R}(x) = \{y \in \mathcal{Y} : s(x, y) \leq \hat{q}\}. \quad (2)$$

If the random pair (X, Y) is exchangeable with \mathcal{D}_{cal} and s is deterministic, SCP guarantees marginal coverage, defined as:

$$\mathbb{P}_{X, Y, \mathcal{D}_{\text{cal}}}(Y \in \hat{R}(X)) = \mathbb{P}(s(X, Y) \leq \hat{q}) \geq 1 - \alpha, \quad (3)$$

where the probability is taken over (X, Y) and \mathcal{D}_{cal} . Assuming no ties in scores, the marginal coverage is exactly $\frac{k_\alpha}{|\mathcal{D}_{\text{cal}}| + 1}$, yielding $\mathbb{P}(Y \in \hat{R}(X)) \leq 1 - \alpha + \frac{1}{|\mathcal{D}_{\text{cal}}| + 1}$.

Ideally, the prediction region should account for heteroskedasticity in the data by achieving *conditional*

coverage at the level $1 - \alpha$, which is defined as:

$$\mathbb{P}(Y \in \hat{R}(X) \mid X = x) \geq 1 - \alpha \quad \forall x \in \mathcal{X}. \quad (4)$$

This is a stronger requirement than marginal coverage in (3). However, as Barber et al. (2019) demonstrate, achieving conditional coverage is generally impossible without making additional assumptions about the underlying data-generating process.

2.2 Multi-output conformal methods

Many conformal prediction methods have been proposed in the literature and implemented within the SCP framework for various base predictors and conformity scores, with a specific focus on univariate prediction problems. In this section, we survey several conformal methods for constructing multivariate prediction regions, using different multivariate base predictors and corresponding conformity scores. Specifically, we discuss three types of methods: marginal-based, density-based, and sample-based, which are based on the marginal distribution of each output variable, their joint probability density function, or a sampling procedure (e.g., a generative model), respectively. In the following, we describe the conformity scores s for each method. Once a conformity score is defined, the corresponding prediction region \hat{R} can be computed using (2). We detail this relation for each method in the Appendix J of the supplementary material. Additionally, in Section 4, we examine the properties and relationships between these methods and provide illustrative examples of the resulting prediction regions.

M-CP. Zhou et al., 2024b applied a univariate conformal method to each output $i \in [d]$ of the multivariate response. Specifically, given a conformity score s_i for the i -th dimension, joint coverage across all dimensions can be achieved using the following conformity score:

$$s_{\text{M-CP}}(x, y) = \max_{i \in [d]} s_i(x, y_i). \quad (5)$$

A similar score has been considered by Diquigiovanni et al. (2023) in the context of functional regression.

In this work, we use Conformalized Quantile Regression (CQR, Romano et al., 2019) for each output $i \in [d]$, where the conformity score is given by:

$$s_i(x, y_i) = \max\{\hat{l}_i(x) - y_i, y_i - \hat{u}_i(x)\},$$

with $\hat{l}_i(x)$ and $\hat{u}_i(x)$ representing the lower and upper conditional quantiles of $Y_i \mid X = x$ at levels α_l and α_u , respectively. In our experiments, we consider equal-tailed prediction intervals, where $\alpha_l = \frac{\alpha}{2}$, $\alpha_u = 1 - \frac{\alpha}{2}$, and α denotes the miscoverage level. The corresponding prediction region $\hat{R}_{\text{M-CP}}(x) = \times_{i=1}^d [\hat{l}_i(x) - \hat{q}, \hat{u}_i(x) + \hat{q}]$ is a hyperrectangle.

DR-CP. Given a predictive density $\hat{f}(y \mid x)$, Sadinle et al. (2016) defines a conformity score as the negative density:

$$s_{\text{DR-CP}}(x, y) = -\hat{f}(y \mid x). \quad (6)$$

The corresponding prediction region is a density super-level set, $\hat{R}_{\text{DR-CP}}(x) = \{y \in \mathcal{Y} : \hat{f}(y \mid x) \geq -\hat{q}\}$.

HDR-CP. With a predictive density $\hat{f}(y \mid x)$, Izbicki et al., 2022 proposed the HPD-split method, which defines a conformity score based on the Highest Predictive Density (HPD):

$$\begin{aligned} \text{HPD}_{\hat{f}}(y \mid x) &= \int_{\{y' \mid \hat{f}(y' \mid x) \geq \hat{f}(y \mid x)\}} \hat{f}(y' \mid x) dy' \quad (7) \\ &= \mathbb{P}\left(\hat{f}(\hat{Y} \mid x) \geq \hat{f}(y \mid x) \mid X = x\right), \quad (8) \end{aligned}$$

where $\hat{Y} \sim \hat{f}(\cdot \mid X)$. The corresponding prediction region is a highest density region (HDR, Hyndman, 1996) with respect to \hat{f} at level \hat{q} :

$$\hat{R}_{\text{HDR-CP}}(x) = \{y \in \mathcal{Y} : \hat{f}(y \mid x) \geq t_{\hat{q}}\}, \quad (9)$$

$$\text{where } t_{\hat{q}} = \sup\{t : \mathbb{P}(\hat{f}(\hat{Y} \mid x) \geq t \mid X = x) \geq \hat{q}\}. \quad (10)$$

Compared to DR-CP, where the threshold $-\hat{q}$ is independent of x , HDR-CP allows the threshold $t_{\hat{q}}$ to vary with x . To compute the HPD in (7), Izbicki et al., 2022 use numerical integration, whereas in our experiments, we approximate (8) using Monte Carlo sampling, as described in (15).

Finally, in the context of classification, Adaptive Prediction Sets (Romano et al., 2020) follows a similar principle by constructing a ‘‘highest mass region’’, which corresponds to a superlevel set of the probability mass function with probability content at least \hat{q} .

PCP. Let $\tilde{Y}^{(1)}, \tilde{Y}^{(2)}, \dots, \tilde{Y}^{(L)}$ denote a sample with L points from the (estimated) conditional distribution $\hat{F}_{Y \mid x}$. Probabilistic Conformal Prediction (PCP, Wang et al., 2023b) defines the conformity score as the distance to the closest point:

$$s_{\text{PCP}}(x, y) = \min_{l \in [L]} \|y - \tilde{Y}^{(l)}\|_2, \quad (11)$$

$$\text{where } \tilde{Y}^{(l)} \sim \hat{F}_{Y \mid x}, \quad l \in [L]. \quad (12)$$

The corresponding region is a union of L balls centered at each sample, i.e. $\hat{R}_{\text{PCP}}(x) = \bigcup_{l \in [L]} \{y \in \mathcal{Y} : \|y - \tilde{Y}^{(l)}\|_2 \leq \hat{q}\}$.

HD-PCP. When a predictive density is available alongside a sample of L points, Wang et al., 2023b proposed an extension to PCP, called HD-PCP. This method

uses the same conformity score as in (11), and retains only the $\lfloor (1 - \alpha)L \rfloor$ samples with the highest density, ensuring that the prediction region is concentrated on high-density points.

ST-DQR. Motivated by the limitation that existing multivariate quantile regression methods do not allow the construction of regions with arbitrary shapes, Feldman et al., 2023 proposed to construct convex regions in a latent space \mathcal{Z} using directional quantile regression (Paindaveine and Šiman, 2011). These regions are then mapped to the output space \mathcal{Y} using a conditional variational autoencoder (CVAE), allowing a non-linear mapping between the two spaces. They further apply a conformalization step by creating a grid of samples in the latent space \mathcal{Z} , mapping samples from region in the latent space to the output space \mathcal{Y} , and constructing d -balls around the mapped samples, similarly to PCP.

3 NEW MULTI-OUTPUT CONFORMAL METHODS

In this section, we introduce two new classes of conformity scores: CDF-based and latent-based. For the former, we propose a specific instance that builds on PCP from Wang et al., 2023b and HPD-split from Izbicki et al., 2020. The latter is inspired by Feldman et al., 2023 and can be interpreted as an extension of distributional conformal prediction (Chernozhukov et al., 2021) for multivariate outputs. Section 4 presents a comparative study of the different conformity scores introduced in Section 2.2 and those introduced in this section.

3.1 CDF-based conformity scores

Consider any conformal method with a conformity score s_W , and define the random variable $W = s_W(X, Y)$ for a random pair (X, Y) . For an observation (x, y) , we introduce a new conformity score based on the cumulative distribution function (CDF) of W conditional on $X = x$, evaluated at $s_W(x, y)$. This is expressed as:

$$\begin{aligned} s_{\text{CDF}}(x, y) &= \mathbb{P}(s_W(X, Y) \leq s_W(x, y) \mid X = x) \quad (13) \\ &= F_{W|X=x}(s_W(x, y) \mid X = x). \quad (14) \end{aligned}$$

This new conformity score measures the rank of $s_W(x, y)$ relative to the distribution of W conditional on $X = x$.

This method applies to any conformity score s_W and generalizes the (oracle) HPD-split introduced in Izbicki et al., 2020. Specifically, when $s_W(x, y) = s_{\text{DR-CP}}(x, y)$ is used in (14), we recover the HDR-CP method. Additionally, by applying the probability integral transform, $s_{\text{CDF}}(X, Y) \mid X = x \sim \mathcal{U}(0, 1)$ for $x \in \mathcal{X}$, meaning that

the conformity score’s distribution is independent of x . This property ensures that conditional coverage is achieved as $\mathcal{D}_{\text{cal}} \rightarrow \infty$ (see Appendix D.2, Lemma 2). A similar observation was made by Izbicki et al., 2020 for HDR-CP.

However, in practice, since the distribution of $Y \mid X = x$ is unknown, s_{CDF} is approximated using Monte Carlo sampling as follows:

$$s_{\text{ECDF}}(x, y) = \frac{1}{K} \sum_{k \in [K]} \mathbb{I}(s_W(x, \hat{Y}^{(k)}) \leq s_W(x, y)),$$

where $\hat{Y}^{(k)} \sim \hat{F}_{Y|x}$, $k \in [K]$. (15)

Dheur et al., 2024 considered a particular case of this empirical CDF-based approach with the $s_{\text{DR-CP}}$ score for a bivariate prediction problem involving temporal point processes, where the HPD region is estimated via Monte Carlo sampling.

C-PCP. We introduce a useful special case of our new score, called C-PCP, by setting $s_W(x, y) = s_{\text{PCP}}(x, y)$ in (15), which gives:

$$s_{\text{C-PCP}}(x, y) = \frac{1}{K} \sum_{k \in [K]} \mathbb{I}\left(\min_{l \in [L]} \|\hat{Y}^{(k)} - \tilde{Y}^{(l)}\| \leq \min_{l \in [L]} \|y - \tilde{Y}^{(l)}\|\right).$$

Compared to the methods in Izbicki et al., 2020 and Dheur et al., 2024, this score has the advantage of not requiring the estimation of a predictive density, relying instead on samples from the conditional distribution. Consequently, this score can be applied with any generative model that does not have an explicit density, while still retaining the desirable properties of our score in (14).

Interestingly, C-PCP shares similarities with the recently proposed CP²-PCP method by Plassier et al., 2024. For a given $x \in \mathcal{X}$, both methods adapt the radius of the prediction balls based on a second sample of K instances conditioned on x , requiring a total of $L + K$ samples. A detailed discussion can be found in Appendix I of the supplementary material.

3.2 Latent-based conformity scores

Inspired by Feldman et al. (2023), we propose a latent-based conformity score with key distinctions. First, our method does not require the use of directional quantile regression. Additionally, the conformalization step is performed directly in the latent space, eliminating the need to construct a grid, which improves both computational efficiency and scalability.

Our base predictor is a conditional invertible generative model $\hat{Q} : \mathcal{Z} \times \mathcal{X} \rightarrow \mathcal{Y}$, which maps a latent

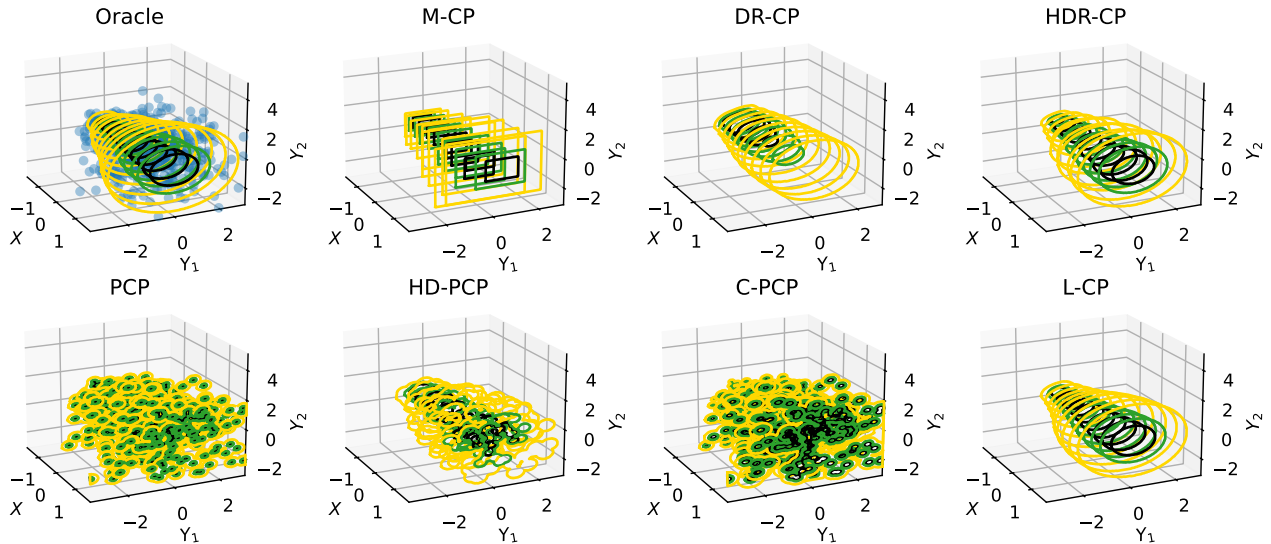


Figure 2: Prediction regions for a bivariate unimodal dataset, conditional on a unidimensional input. The black, green, and yellow contours represent regions with nominal coverage levels of 20%, 40%, and 80%, respectively.

random variable $Z \in \mathcal{Z}$ (e.g., drawn from a standard multivariate normal distribution) to the output space \mathcal{Y} , conditional on input $X \in \mathcal{X}$ (e.g., using normalizing flows). The model is both conditional and invertible, meaning that $\hat{Q}(\hat{Q}^{-1}(y; x); x) = y, \forall x \in \mathcal{X}, y \in \mathcal{Y}$.

We propose the following conformity score, called **L-CP**, defined as:

$$s_{\text{L-CP}}(x, y) = d_{\mathcal{Z}}(\hat{Q}^{-1}(y; x)),$$

where $d_{\mathcal{Z}} : \mathcal{Z} \rightarrow \mathbb{R}$ is a conformity function in the latent space \mathcal{Z} , independent of x . In our experiments, we use $Z \sim \mathcal{N}(0, I_d)$ and $d_{\mathcal{Z}}(z) = \|z\|$.

The corresponding prediction region is obtained by mapping a region in the latent space, $R_{\mathcal{Z}}(\hat{q}) = \{z \in \mathcal{Z} : d_{\mathcal{Z}}(z) \leq \hat{q}\}$, to a region in the output space, $\hat{R}_{\text{L-CP}}(x) = \{\hat{Q}(z; x) : z \in R_{\mathcal{Z}}(\hat{q})\}$.

L-CP generalizes Distributional Conformal Prediction (Chernozhukov et al., 2021), which is a special case when Y is univariate ($d = 1$), $Z \sim \mathcal{U}(0, 1)$, $d_{\mathcal{Z}}(z) = |z - \frac{1}{2}|$, and $\hat{Q}(\cdot; x)$ is the quantile function of Y given x .

4 COMPARISON OF MULTI-OUTPUT CONFORMAL METHODS

This section compares the different multi-output conformal methods discussed in the previous sections, including illustrative examples. We then highlight the differences between the existing and proposed multivariate conformal methods presented in Sections 2.2 and 3, evaluating them based on various properties.

4.1 Illustrative examples

We provide illustrative examples of bivariate prediction regions for different conformal methods on simulated data, covering both unimodal (Figure 2) and bimodal distributions (Figure 5 in Appendix B.1). The data generating processes are detailed in Appendix B.1. Additionally, we present bivariate prediction regions for a real-world application, predicting a taxi passenger’s drop-off location based on the passenger’s information (Figures 6 and 7 in Appendix B.2).

In both Figures 2 and 5, the black, green, and yellow contours represent prediction regions with nominal coverage levels of 20%, 40%, and 80%, respectively. The top-left panel illustrates the density level sets of the oracle distribution $F_{Y|X}$. The remaining panels display the prediction regions generated by various conformal methods, all utilizing the MQF² base predictor, as detailed in Appendix A.2.

We observe the following for the unimodal case in Figure 2. **M-CP** captures heteroscedasticity but produces rectangular prediction regions, which do not conform to the circular level sets of $Y | X$, resulting in a lack of sharpness. **DR-CP** fails to maintain conditional coverage, and for $X = 1$, the absence of black and green contours suggests that the predictive density does not reach the threshold $-\hat{q}$ defined in (6) for coverage levels of 0.2 or 0.4. **HDR-CP** generates prediction regions that are relatively close to the level sets of $Y | X$, though the contours are noisy due to sampling uncertainty as described in (15). **PCP** generates highly discontinuous regions, especially at lower coverage levels, where the regions appear as balls centered on individual samples.

Table 1: Comparison of multivariate conformal methods according to various criteria. (*) **M-CP** achieves asymptotic conditional coverage under certain assumptions (see Appendix D.2.3). (**) While **L-CP** does not require evaluating the predictive density, computing the scores and regions requires calculating the inverse transformation of the quantile function \hat{Q}^{-1} .

Method	Type of region	Asymptotic conditional coverage	Small average size	Low compute time	Predictive density not required	Sampling procedure not required
M-CP	Union of hyperrectangles	✓(*)	***	****	✓	✓
DR-CP	Density superlevel set	✗	***	****	✗	✓
HDR-CP	Highest density region	When $K \rightarrow \infty$	***	****	✗	✗
PCP	Union of d -balls	✗	***	****	✓	✗
HD-PCP	Union of d -balls	✗	***	****	✗	✗
C-PCP	Union of d -balls	When $K \rightarrow \infty$	***	****	✓	✗
L-CP	Quantile region	✓	***	****	✓(**)	✗

In contrast, **HD-PCP** produces more continuous regions but requires knowledge of the density function f .

For our methods, unlike **PCP**, **C-PCP** adjusts the radius of the prediction regions to improve conditional coverage. This is evident in the example, where the radius of the balls for $X = -1$ is smaller than for $X = 1$, as indicated by the tighter regions around the samples. **L-CP** generates prediction regions that closely align with the true level sets of $Y | X$, demonstrating good conditional coverage.

For the bimodal distribution in Figure 5 (Appendix B.1), the prediction regions generated by **M-CP** and **L-CP** are connected, failing to capture the bimodal nature of the distribution. In the real-world application, Figures 6 and 7 (Appendix B.2) illustrate predictions under low and high uncertainty, respectively. Our methods, **L-CP** and **C-PCP**, alongside **M-CP** and **HDR-CP**, demonstrate the best adaptability to outputs with varying levels of uncertainty.

4.2 Properties

In this section, we compare conformal methods based on several key properties. While all the conformal methods presented achieve the classical conformal *marginal coverage*, as noted by Wang et al., 2023b (Theorem 1), the marginal coverage of methods such as **HDR-CP**, **PCP**, **HD-PCP**, and **C-PCP** also depends on the randomness of the generated samples. Additionally, in Appendix D.1, we demonstrate that the marginal coverage, conditional on the calibration dataset \mathcal{D}_{cal} and the samples drawn from it, follows a beta distribution, using standard arguments. Throughout this analysis, we use $\stackrel{d}{=}$ to denote equality in distribution and $\stackrel{\text{a.s.}}{=}$ to denote almost sure equality.

We first examine the *asymptotic conditional coverage*

(ACC) property, which corresponds to conditional coverage as defined in (4), under the following conditions:

1. The base predictor corresponds to the oracle distribution $F_{Y|X}$. Specifically, for **M-CP**, $\hat{l}_i(x) = Q_{Y_i}(\alpha_l | x)$ and $\hat{u}_i(x) = Q_{Y_i}(\alpha_u | x)$; for **DR-CP**, **HDR-CP**, and **HD-PCP**, $\hat{f}(\cdot | X) = f_{Y|X}$; for **L-CP**, $\hat{Q}(Z|X) \stackrel{d}{=} Y|X$; and for **PCP** and **C-PCP**, $\hat{F}_{Y|X} = F_{Y|X}$.
2. As $|D_{\text{cal}}| \rightarrow \infty$, \hat{q} converges to the $1 - \alpha$ quantile of the random variable $s(X, Y)$.

L-CP achieves ACC without additional assumptions, while **HDR-CP** and **C-PCP** achieve ACC with $K \rightarrow \infty$. **M-CP** achieves ACC under specific assumptions. Assuming that Y_1, \dots, Y_d are conditionally independent given X , **M-CP** achieves ACC if $\alpha_u - \alpha_l = \sqrt[d]{1 - \alpha}$. Furthermore, under the assumption that $Y_1 | X \stackrel{\text{a.s.}}{=} \dots \stackrel{\text{a.s.}}{=} Y_d | X$, **M-CP** achieves ACC if $\alpha_u - \alpha_l = 1 - \alpha$. The true dependence typically lies between these two extremes. We provide detailed proofs of these statements in Appendix D.2.

As discussed in Section 4.1, **DR-CP** fails to achieve ACC. Likewise, **PCP** and **HD-PCP** do not achieve ACC, as they are constrained to producing regions with limited volume, conditional on any $x \in \mathcal{X}$. Assuming each ball has a volume of V , **PCP** generates a region with a total volume of at most LV . When $Y | X = x$ has high uncertainty, it may be impossible to capture sufficient probability mass with a volume restricted to LV .

In terms of average region size, **DR-CP** performs best, as it minimizes $\mathbb{E}[|R(X)|]$, as demonstrated in Theorem 1 by Sadinle et al., 2016. On the other hand, **M-CP** is expected to output larger regions since it does not account for dependencies between outputs. When the region $R_Z(\lambda)$ in the latent space is connected for all $\lambda \in \mathbb{R}$ and

\hat{Q} is continuous, L-CP cannot handle multimodality because it is restricted to connected regions. While PCP, HD-PCP, and C-PCP can handle multimodality, they are susceptible to the curse of dimensionality, as they rely on a finite union of balls. In high-dimensional spaces, where data becomes sparse, larger balls are needed to achieve marginal coverage

In terms of computational time, HDR-CP, PCP, HD-PCP, and C-PCP are significantly slower than M-CP, L-CP, and DR-CP since they need to generate a large number of samples to compute the conformity score or region (we used $K = L = 100$ in our experiments).

Finally, certain methods stand out because they do not need to evaluate the predictive density \hat{f} or generate samples. M-CP only requires a univariate model for the distribution of each output Y_i , without needing a model for the joint distribution of Y . DR-CP does not require sampling from the model, which is beneficial when using some normalizing flows that are slower to invert, such as Masked Autoregressive Flows (MAF, Papamakarios, Pavlakou, et al., 2017) or Convex Potential Flows (Huang et al., 2020). PCP and C-PCP do not require evaluating the predictive density \hat{f} , making them compatible with any generative model, including diffusion models and GANs. L-CP does not require predictive density evaluation but does require the model to be invertible. We summarize the comparisons in Table 1.

4.3 Connection between sample-based and density-based methods

Interestingly, the sample-based methods (PCP, HD-PCP, C-PCP) can be viewed as special cases of density-based methods (DR-CP, HDR-CP).

Let us assume a common density function \hat{f} is used for the base predictor in these conformal methods. While PCP and C-PCP do not require knowledge of a density function, we assume that $\hat{f}(\cdot | x)$ and $\hat{F}_{Y|x}$ correspond to the same distribution. Let $\tilde{Y}^{(l)} \sim \hat{F}_{Y|x}$ for $l \in [L]$, and $f_{\mathbb{S}}(\cdot; \tilde{Y}^{(l)})$ be a density function with spherical level sets, centered at $\tilde{Y}^{(l)}$, such as a standard multivariate Gaussian $\mathcal{N}(\cdot; \tilde{Y}^{(l)}, I_d)$. For $x \in \mathcal{X}$, we define a new density function $\hat{f}_{\max}(y | x) = \max_{l \in [L]} f_{\mathbb{S}}(y; \tilde{Y}^{(l)})/C$, where C is a normalization constant ensuring that $\hat{f}_{\max}(\cdot | x)$ integrates to 1. The following proposition establishes the relationship between these methods.

Proposition 1. PCP is equivalent to DR-CP with $\hat{f} = \hat{f}_{\max}$. Similarly, HD-PCP is equivalent to DR-CP with $\hat{f} = \hat{f}_{\max}$ where only $\lfloor (1 - \alpha)L \rfloor$ samples with the highest density among $\{\tilde{Y}^{(l)}\}_{l \in [L]}$ are kept. Finally, C-PCP is equivalent to HDR-CP with $\hat{f} = \hat{f}_{\max}$.

We provide a proof in Appendix D.3. Although these

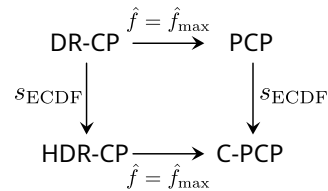


Figure 3: Summary of the connections between different conformal methods.

sample-based methods are special cases of density-based approaches, the key advantage of PCP and C-PCP is that they rely solely on a sampling procedure, without requiring a predictive density \hat{f} as base predictor. Figure 3 summarizes the connections between the main conformal methods.

5 RELATED WORK

Conformal Prediction (CP), introduced by Vovk et al., 1999, forms the foundation of our work by providing prediction regions with finite-sample coverage guarantees. While CP methods are well-established for univariate regression (Papadopoulos et al., 2008; Lei and Wasserman, 2014; Romano et al., 2019; Sesia and Romano, 2021) and classification (Romano et al., 2020; Angelopoulos et al., 2020), extending them to high-dimensional outputs poses challenges. Recent applications in image processing (Horwitz and Hoshen, 2022; Teneggi et al., 2023) apply CP in a pixel-wise manner, resulting in hyperrectangular regions that may not capture pixel dependencies effectively.

To address multivariate prediction challenges, optimal transport methods like cyclically monotone mappings (Carlier et al., 2016) define multivariate quantiles with desirable properties such as existence and uniqueness of mappings. These approaches have been refined by Hallin and Šiman, 2017; Hallin et al., 2021 and adapted for conditional tasks by Barrio et al., 2022. Neural network-based techniques leverage normalizing flows (Kan et al., 2022; Huang et al., 2020) or variational autoencoders (Feldman et al., 2023) to learn flexible, non-convex quantile regions. Additionally, conformalized highest density regions (HDRs) (Hyndman, 1996) handle multimodality and have been applied in various contexts (Camehl et al., 2024; Izbicki et al., 2022; Dheur et al., 2024). Recently, Wang et al., 2023b proposed constructing prediction regions as hyperballs centered on generative model samples, with extensions by Plassier et al., 2024 improving conditional validity.

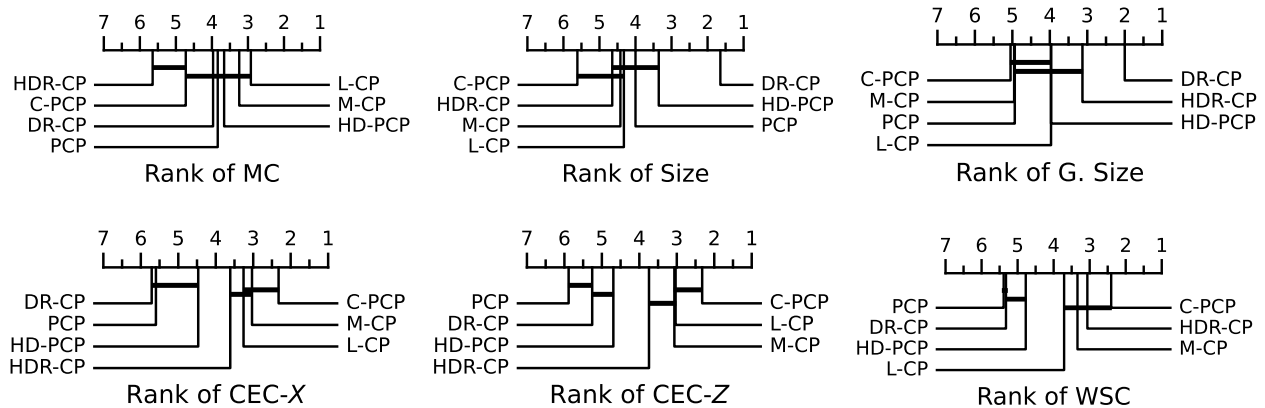


Figure 4: CD diagrams with the base predictor MQF^2 based on 10 runs per dataset and method.

6 A LARGE-SCALE STUDY OF MULTI-OUTPUT CONFORMAL METHODS

In this section, we conduct a large-scale study of multi-output conformal methods based on a total of 32 tabular datasets considered in previous studies (Tsoumakas et al., 2011; Feldman et al., 2023; Cevid et al., 2022; Wang et al., 2023b; Barrio et al., 2022; Camehl et al., 2024). The number of data points n in these datasets ranges from 103 to 50,000, with the number of inputs p ranging from 1 to 348, and the number of outputs d ranging from 2 to 16.

The results presented here are based on the Multivariate Quantile Function Forecaster (MQF^2 , Kan et al., 2022), which is a normalizing flow. We evaluate the methods using several metrics, including marginal coverage (MC), mean region size (Size), the logarithm of the geometric mean of the region size (G. Size), and three metrics for conditional coverage (WSC, CEC-X, and CEC-V). We provide a detailed description of the experimental setup in Appendix A.

Figure 4 presents critical difference (CD) diagrams for the 32 datasets, using the MQF^2 model and the metrics described in Appendices A.1 to A.3. Methods with a lower rank (further to the right) indicate a better performance. Thick horizontal lines connect models whose performance are not statistically different at the 0.05 significance level (see Appendix A.4 for more details). All methods achieve similar marginal coverage, which is expected since marginal coverage follows the same beta distribution for all methods (see Lemma 1 in Appendix D.1).

DR-CP achieves a significantly smaller mean region size, which aligns with expectations since it minimizes $\mathbb{E}[|\hat{R}(X)|]$. While **HDR-CP** results in a large mean region size, the geometric mean of the region sizes is small, in-

dicating **HDR-CP** sometimes produces larger regions due to its adaptiveness, but this effect is less pronounced when considering the geometric mean. **M-CP**, **L-CP**, **C-PCP**, and **HDR-CP** have better conditional coverages according to the WSC, CEC-X, and CEC-V metrics, without significant difference between them. Recall that they achieve asymptotic conditional coverage under specific conditions (see Section 4.2).

Computation time is discussed in Appendix G. **L-CP** and **DR-CP** have the smallest computation times, as they do not require sampling for each calibration and test instance. **M-CP** would also achieve a low computation time if it were not dependent on samples from MQF^2 (see Appendix A.2). Detailed results are available in Appendix H.

Appendix E provides additional results for a conditional normalizing flow on the CIFAR-10 dataset, where similar conclusions are drawn for all methods.

7 CONCLUSION

We conducted a unified comparative study to evaluate several conformal methods for multi-output regression. The tested methods are either based on the marginal distribution of each output variable or on their joint distribution. Methods encompass both density-based and sample-based cases. We introduced two conformity scores with asymptotic conditional coverage: **C-PCP**, compatible with any generative model, and **L-CP**, computationally efficient using an invertible model. We highlighted their respective strengths and weaknesses. Finally, we conducted a comprehensive empirical study to compare all the multi-output conformal methods considered in this work.

Given the generality of the presented methodologies, future directions of research should focus on extensions of these methodologies on more complex outputs such

as semi-structured or unstructured data (e.g. images, text, or graphs) or structured data with constraints, living in less-standard mathematical embeddings (e.g. compositional data, uni- and multi- variate probability distributions, variance-covariance matrices).

Investigating finite-sample conditional guarantees, as in Plassier et al., 2024, is another potential direction. Our methods are also compatible with conformal risk control (Angelopoulos et al., 2024), allowing for extensions to other risks beyond marginal coverage.

References

- [1] Brandon Amos, Lei Xu, and J Zico Kolter. “Input Convex Neural Networks”. In: *Proceedings of the 34th International Conference on Machine Learning*. Ed. by Doina Precup and Yee Whye Teh. Vol. 70. Proceedings of Machine Learning Research. PMLR, 2017, pp. 146–155.
- [2] Anastasios N Angelopoulos and Stephen Bates. “A Gentle Introduction to Conformal Prediction and Distribution-Free Uncertainty Quantification”. *arXiv [cs.LG]* (July 2021). eprint: 2107.07511 (cs.LG).
- [3] Anastasios Nikolas Angelopoulos et al. “Conformal Risk Control”. In: *The Twelfth International Conference on Learning Representations*. 2024.
- [4] Anastasios Nikolas Angelopoulos et al. “Uncertainty Sets for Image Classifiers using Conformal Prediction”. In: *International Conference on Learning Representations*. Oct. 2, 2020.
- [5] Rina Foygel Barber et al. “The limits of distribution-free conditional predictive inference”. *arXiv [math.ST]* (Mar. 11, 2019). eprint: 1903.04684 (math.ST).
- [6] Eustasio del Barrio, Alberto Gonzalez Sanz, and Marc Hallin. “Nonparametric Multiple-Output Center-Outward Quantile Regression”. *arXiv [stat.ME]* (Apr. 25, 2022). eprint: 2204.11756 (stat.ME).
- [7] Alessio Benavoli, Giorgio Corani, and Francesca Mangili. “Should We Really Use Post-Hoc Tests Based on Mean-Ranks?”. *Journal of machine learning research: JMLR* 17 (5 2016), pp. 1–10.
- [8] Christopher M Bishop. *Mixture density networks*. Tech. rep. Birmingham, 1994.
- [9] Annika Camehl, Dennis Fok, and Kathrin Gruber. “On superlevel sets of conditional densities and multivariate quantile regression”. en. *Journal of Econometrics* (105807 July 4, 2024), p. 105807.
- [10] Guillaume Carlier, Victor Chernozhukov, and Alfred Galichon. “Vector quantile regression: An optimal transport approach”. en. *Annals of statistics* 44 (3 June 1, 2016), pp. 1165–1192.
- [11] Maxime Cauchois, Suyash Gupta, and John C Duchi. “Knowing what you know: valid and validated confidence sets in multiclass and multilabel prediction”. *Journal of machine learning research: JMLR* 22 (1 Jan. 1, 2021), pp. 3681–3722.
- [12] Domagoj Cevic et al. “Distributional Random Forests: Heterogeneity Adjustment and Multivariate Distributional Regression”. *Journal of machine learning research: JMLR* 23 (333 2022), pp. 1–79.
- [13] Victor Chernozhukov, Kaspar Wüthrich, and Yinchu Zhu. “Distributional conformal prediction”. en. *Proceedings of the National Academy of Sciences of the United States of America* 118 (48 Nov. 2021).
- [14] Janez Demšar. “Statistical Comparisons of Classifiers over Multiple Data Sets”. *Journal of machine learning research: JMLR* 7 (Dec. 2006), pp. 1–30.
- [15] Victor Dheur et al. “Distribution-Free Conformal Joint Prediction Regions for Neural Marked Temporal Point Processes”. *arXiv [cs.LG]* (Jan. 9, 2024). eprint: 2401.04612 (cs.LG).
- [16] Jacopo Diquigiovanni, Matteo Fontana, and Simone Vantini. “Conformal prediction bands for multivariate functional data”. en. *J. Multivar. Anal.* 189.104879 (May 2022), p. 104879.
- [17] Jacopo Diquigiovanni, Matteo Fontana, and Simone Vantini. “Distribution-free prediction bands for multivariate functional time series: An application to the Italian gas market”. *arXiv [stat.ME]* (July 2021).
- [18] Jacopo Diquigiovanni, Matteo Fontana, and Simone Vantini. “The Importance of Being a Band: Finite-Sample Exact Distribution-Free Prediction Sets for Functional Data”. *Statistica Sinica* SS-2022-0087 (2023).
- [19] Eshant English et al. “JANET: Joint Adaptive predictionN-region Estimation for time-series”. *arXiv [stat.ML]* (July 8, 2024). eprint: 2407.06390 (stat.ML).
- [20] Shai Feldman, Stephen Bates, and Yaniv Romano. “Calibrated Multiple-Output Quantile Regression with Representation Learning”. *Journal of machine learning research: JMLR* 24 (24 2023), pp. 1–48.
- [21] Milton Friedman. “A Comparison of Alternative Tests of Significance for the Problem of m Rankings”. en. *The Annals of Mathematical Statistics* 11 (1 Mar. 1940), pp. 86–92.
- [22] Léo Grinsztajn, Edouard Oyallon, and Gaël Varoquaux. “Why do tree-based models still outperform deep learning on tabular data?” *arXiv [cs.LG]* (July 2022). eprint: 2207.08815 (cs.LG).
- [23] David Ha, Andrew M Dai, and Quoc V Le. “HyperNetworks”. In: *International Conference on Learning Representations*. July 21, 2022.
- [24] Marc Hallin and Miroslav Šiman. “Multiple-output quantile regression”. *Handbook of quantile regression* (2017), pp. 185–207.
- [25] Marc Hallin et al. “Distribution and quantile functions, ranks and signs in dimension d : A measure transportation approach”. en. *The Annals of Statistics* 49 (2 Apr. 2021), pp. 1139–1165.
- [26] Sture Holm. “A Simple Sequentially Rejective Multiple Test Procedure”. *Scandinavian journal of statistics, theory and applications* 6 (2 1979), pp. 65–70.
- [27] Elisha Horwitz and Yedid Hoshen. “Confusion: Confidence Intervals for Diffusion Models”. *arXiv [cs.CV]* (Nov. 17, 2022). eprint: 2211.09795 (cs.CV).
- [28] Chin-Wei Huang et al. “Convex Potential Flows: Universal Probability Distributions with Optimal Transport and Convex Optimization” (Oct. 2, 2020).
- [29] Rob J Hyndman. “Computing and Graphing Highest Density Regions”. *The American statistician* 50 (2 1996), pp. 120–126.
- [30] Rafael Izbicki, Gilson Shimizu, and Rafael Stern. “Flexible distribution-free conditional predictive bands using density estimators”. In: *Proceedings of the Twenty Third International Conference on Artificial Intelligence and Statistics*. Ed. by Silvia Chiappa and Roberto Calandra. Vol. 108. Proceedings of Machine Learning Research. PMLR, 2020, pp. 3068–3077.
- [31] Rafael Izbicki, Gilson Shimizu, and Rafael B Stern. “CD-split and HPD-split: Efficient Conformal Regions in High Dimensions”. *Journal of machine learning research: JMLR* 23 (87 2022), pp. 1–32.

- [32] Chancellor Johnstone and Eugene Ndiaye. “Exact and approximate conformal inference for multi-output regression”. *arXiv [stat.ML]* (Oct. 2022).
- [33] Kelvin Kan et al. “Multivariate Quantile Function Forecaster”. In: *Proceedings of The 25th International Conference on Artificial Intelligence and Statistics*. Ed. by Gustau Camps-Valls, Francisco J R Ruiz, and Isabel Valera. Vol. 151. Proceedings of Machine Learning Research. PMLR, 2022, pp. 10603–10621.
- [34] Durk P Kingma and Prafulla Dhariwal. “Glow: Generative Flow with Invertible 1x1 Convolutions”. In: *Advances in Neural Information Processing Systems*. Ed. by S Bengio et al. Vol. 31. Curran Associates, Inc., 2018.
- [35] Alex Krizhevsky, Vinod Nair, Geoffrey Hinton, et al. “The CIFAR-10 dataset”. *online: http://www.cs.toronto.edu/kriz/cifar.html* 55 (5 2014), p. 2.
- [36] Jing Lei and Larry Wasserman. “Distribution-free prediction bands for non-parametric regression”. en. *Journal of the Royal Statistical Society. Series B, Statistical methodology* 76 (1 Jan. 2014), pp. 71–96.
- [37] S Messoudi. “Ellipsoidal conformal inference for Multi-Target Regression”. *COPA* (2022), pp. 294–306.
- [38] Soundouss Messoudi, Sébastien Destercke, and Sylvain Rousseau. “Copula-based conformal prediction for Multi-Target Regression”. *arXiv [cs.LG]* (Jan. 2021).
- [39] Eric Nalisnick et al. “Do Deep Generative Models Know What They Don’t Know?” In: *International Conference on Learning Representations*. Sept. 27, 2018.
- [40] Davy Paindaveine and Miroslav Šiman. “On directional multiple-output quantile regression”. en. *Journal of multivariate analysis* 102 (2 Feb. 1, 2011), pp. 193–212.
- [41] Harris Papadopoulos, Alex Gammerman, and Volodya Vovk. “Normalized nonconformity measures for regression Conformal Prediction”. en. In: *Proceedings of the 26th IASTED International Conference on Artificial Intelligence and Applications* (Innsbruck, Austria). AIA ’08. USA: ACTA Press, Feb. 6, 2008, pp. 64–69.
- [42] Harris Papadopoulos et al. “Inductive Confidence Machines for Regression”. In: *Machine Learning: ECML 2002*. Springer Berlin Heidelberg, 2002, pp. 345–356.
- [43] Papamakarios, Pavlakou, et al. “Masked autoregressive flow for density estimation”. *Advances in neural information processing systems* (2017).
- [44] Ji Won Park, Robert Tibshirani, and Kyunghyun Cho. *Semiparametric conformal prediction*. arXiv:2411.02114. Nov. 2024.
- [45] Vincent Plassier et al. “Conditionally valid Probabilistic Conformal Prediction”. *arXiv [stat.ML]* (July 1, 2024). eprint: 2407.01794 (stat.ML).
- [46] Alvin Rajkomar et al. “Scalable and accurate deep learning with electronic health records”. en. *npj digital medicine* 1 (1 May 8, 2018), p. 18.
- [47] Yaniv Romano, Evan Patterson, and Emmanuel Candès. “Conformalized quantile regression”. *Advances in neural information processing systems* (2019).
- [48] Yaniv Romano, Matteo Sesia, and Emmanuel J Candès. “Classification with valid and adaptive coverage”. *arXiv [stat.ME]* (June 3, 2020). eprint: 2006.02544 (stat.ME).
- [49] Raphael Rossellini, Rina Foygel Barber, and Rebecca Willett. “Integrating Uncertainty Awareness into Conformalized Quantile Regression”. *arXiv [stat.ME]* (June 14, 2023). eprint: 2306.08693 (stat.ME).
- [50] Mauricio Sadinle, Jing Lei, and Larry Wasserman. “Least Ambiguous Set-Valued Classifiers with Bounded Error Levels”. *arXiv [stat.ME]* (Sept. 2, 2016). eprint: 1609.00451 (stat.ME).
- [51] Matteo Sesia and Yaniv Romano. “Conformal prediction using conditional histograms”. *Advances in neural information processing systems* (2021).
- [52] Kamile Stankeviciute, Ahmed M. Alaa, and Mihaela van der Schaar. “Conformal Time-series Forecasting”. In: *Advances in Neural Information Processing Systems*. Ed. by M Ranzato et al. Vol. 34. Curran Associates, Inc., 2021, pp. 6216–6228.
- [53] Vincent Stimper, Bernhard Schölkopf, and Jose Miguel Hernandez-Lobato. “Resampling Base Distributions of Normalizing Flows”. en. In: *International Conference on Artificial Intelligence and Statistics*. International Conference on Artificial Intelligence and Statistics. PMLR, May 3, 2022, pp. 4915–4936.
- [54] Sophia Sun and Rose Yu. “Copula Conformal Prediction for multi-step Time Series forecasting”. *arXiv [cs.LG]* (Dec. 2022).
- [55] Jacopo Teneggi et al. “How to Trust Your Diffusion Model: A Convex Optimization Approach to Conformal Risk Control” (June 15, 2023).
- [56] Alexander Timans et al. *Adaptive Bounding Box Uncertainties via Two-Step Conformal Prediction*. arXiv:2403.07263. July 2024.
- [57] Grigorios Tsoumakas et al. “MULAN: A Java Library for Multi-Label Learning”. *Journal of machine learning research: JMLR* 12 (71 2011), pp. 2411–2414.
- [58] V Vovk, A Gammerman, and C Saunders. “Machine-Learning Applications of Algorithmic Randomness”. en. *International Conference on Machine Learning* (1999).
- [59] Jun Wang et al. *Conformal Temporal Logic Planning using Large Language Models: Knowing When to Do What and When to Ask for Help*. arXiv:2309.10092 [cs]. Dec. 2023.
- [60] Zhendong Wang et al. “Probabilistic Conformal Prediction Using Conditional Random Samples”. en. In: *International Conference on Artificial Intelligence and Statistics*. International Conference on Artificial Intelligence and Statistics. PMLR, Apr. 11, 2023, pp. 8814–8836.
- [61] Frank Wilcoxon. “Individual Comparisons by Ranking Methods”. *Biometrics Bulletin* 1 (6 1945), pp. 80–83.
- [62] Chen Xu, Hanyang Jiang, and Yao Xie. “Conformal prediction for multi-dimensional time series by ellipsoidal sets”. *arXiv [stat.ML]* (Mar. 2024).
- [63] Xiaofan Zhou et al. *Conformal Prediction: A Data Perspective*. arXiv:2410.06494. Oct. 2024.
- [64] Yanfei Zhou, Lars Lindemann, and Matteo Sesia. “Conformalized Adaptive Forecasting of Heterogeneous Trajectories”. *arXiv [stat.ML]* (Feb. 14, 2024). eprint: 2402.09623 (stat.ML).

Checklist

1. For all models and algorithms presented, check if you include:
 - (a) A clear description of the mathematical setting, assumptions, algorithm, and/or model. Yes
 - (b) An analysis of the properties and complexity (time, space, sample size) of any algorithm. [Yes/No/Not Applicable]
 - (c) (Optional) Anonymized source code, with specification of all dependencies, including external libraries. Yes
2. For any theoretical claim, check if you include:
 - (a) Statements of the full set of assumptions of all theoretical results. Yes
 - (b) Complete proofs of all theoretical results. Yes
 - (c) Clear explanations of any assumptions. Yes
3. For all figures and tables that present empirical results, check if you include:
 - (a) The code, data, and instructions needed to reproduce the main experimental results (either in the supplemental material or as a URL). Yes
 - (b) All the training details (e.g., data splits, hyperparameters, how they were chosen). Yes
 - (c) A clear definition of the specific measure or statistics and error bars (e.g., with respect to the random seed after running experiments multiple times). Yes
 - (d) A description of the computing infrastructure used. (e.g., type of GPUs, internal cluster, or cloud provider). Yes
4. If you are using existing assets (e.g., code, data, models) or curating/releasing new assets, check if you include:
 - (a) Citations of the creator If your work uses existing assets. Yes
 - (b) The license information of the assets, if applicable. Yes
 - (c) New assets either in the supplemental material or as a URL, if applicable. Yes
 - (d) Information about consent from data providers/curators. Not Applicable
 - (e) Discussion of sensible content if applicable, e.g., personally identifiable information or offensive content. Not Applicable
5. If you used crowdsourcing or conducted research with human subjects, check if you include:
 - (a) The full text of instructions given to participants and screenshots. [Not Applicable]
 - (b) Descriptions of potential participant risks, with links to Institutional Review Board (IRB) approvals if applicable. Not Applicable
 - (c) The estimated hourly wage paid to participants and the total amount spent on participant compensation. Not Applicable

A Experimental setup

This section describes our experimental setup in more details. Computations were performed based on 2 workstations, one with 2 A6000 GPUs and 64 CPU threads, and one with 2 A5000 GPUs and 64 CPU threads, running for 48 hours.

A.1 Datasets

We consider a total of 32 datasets that have been used in previous studies. Since our focus is on multivariate prediction regions, we select only datasets with an output that is at least two-dimensional. Specifically, we include 17 datasets from Tsoumakas et al., 2011 (MULAN benchmark), 6 datasets from Feldman et al., 2023, 4 datasets from Cevic et al., 2022, 2 datasets from Wang et al., 2023b, 2 datasets from Barrio et al., 2022, and 1 dataset from Camehl et al., 2024.

The number of data points ranges from 103 to 50,000, the number of inputs (features) ranges from 1 to 348, and the number of outputs ranges from 2 to 16. Each dataset is split into training, validation, calibration, and test sets with proportions of 0.4, 0.1, 0.3, and 0.2, respectively. The preprocessing follows the setup described in Grinsztajn et al., 2022. Table 3 in Appendix F provides the detailed characteristics of each dataset.

A.2 Base predictors

We consider multiple base predictors and focus on MQF² for our main experiments (Section 6).

MQF². The Multivariate Quantile Function Forecaster (MQF², Kan et al., 2022) is a normalizing flow that is compatible with all the methods presented (except **M-CP**), as it is invertible, has an explicit density function, and can be sampled from. The quantile function \hat{Q} and distribution function \hat{Q}^{-1} of MQF² exhibit cyclical monotonicity, meaning they are the gradient of a convex function (Hallin et al., 2021).

Since direct estimation of the marginal distributions for each output $Y_i, i \in [d]$ is not feasible with MQF², the lower and upper quantiles for **M-CP** are estimated by first sampling $\{\hat{Y}^{(l)}\}_{l \in [L]}$ from $\hat{f}(\cdot | x)$ given $x \in \mathcal{X}$, and then calculating the empirical quantiles $\hat{Y}_i^{(\lfloor L \frac{\alpha}{2} \rfloor)}$ and $\hat{Y}_i^{(\lfloor L(1-\frac{\alpha}{2}) \rfloor)}$. Although **M-CP** could be paired with a more computationally efficient base predictor, this approach ensures a direct comparison with other conformal methods using the same base predictor.

The main idea behind MQF² is to interpret Convex Potential Flows (Huang et al., 2020) as multivariate (vector) quantile functions, in the sense that the representation property (16) and cyclical monotonicity property (17) are satisfied (Carlier et al., 2016):

$$Y = \hat{Q}(Z; x) \quad \forall x \in \mathcal{X} \text{ where } Z \sim \mathcal{U}(0, 1)^d, \quad (16)$$

$$\left(\hat{Q}(z_1; x) - \hat{Q}(z_2; x) \right)^T (z_1 - z_2) \geq 0 \quad \forall x \in \mathcal{X}, z_1, z_2 \in \mathcal{Z}. \quad (17)$$

When $d = 1$, this reduces to the classical univariate quantile function. In practice, we follow Kan et al., 2022 and use a quantile vector that follows a normal distribution $Z \sim \mathcal{N}(0, I)$, allowing better training.

The underlying model of MQF² is a partially input-convex neural network (PINN, Amos et al., 2017) with two hidden layers, each containing 20 units. Increasing the number of parameters did not significantly improve performance, which is partly due to the efficiency of Convex Potential Flows compared to other normalizing flows (Huang et al., 2020). While hyperparameter tuning for each dataset could enhance performance, it is not the primary focus of this paper.

MQF² is trained using maximum likelihood estimation with early stopping, with a patience of 15 epochs, where validation loss is measured every two epochs.

Distributional Random Forests. Distributional Random Forest (Cevic et al., 2022) is a model built upon the Random Forest algorithm, which adaptively identifies the relevant training data points for any given test point. More specifically, given a test point $x \in \mathcal{X}$, Distributional Random Forest outputs a weight $w(x^{(i)} | x)$ for each training point $x^{(i)}$ with $x^{(i)} \in \mathcal{D}_{\text{train}}$. This approach enables accurate estimation of any quantity of interest

conditional on $x \in \mathcal{X}$. In our experiments, we estimate the conditional distribution $Y|X$ as a Gaussian mixture, with each component centered on a training point and weighted by the Distributional Random Forest.

The density function at $y \in \mathcal{Y}$ given $x \in \mathcal{X}$ is expressed as:

$$\hat{f}(y | x) = \sum_{i=1}^{|\mathcal{D}_{\text{train}}|} w(x^{(i)} | x) \cdot \mathcal{N}(y | y^{(i)}, \sigma I_d),$$

where σ is tuned by minimizing the NLL on a grid search.

Since this method does not operate in a latent space, we do not consider **L-CP** in combination with this base predictor. CD diagrams for this predictor are presented in Appendix C.1.

Multivariate Gaussian Mixture Model parameterized by a hypernetwork. As another base predictor, we consider a multivariate Gaussian Mixture Model parameterized by a hypernetwork. The hypernetwork is a multilayer perceptron (MLP) that outputs the parameters of a mixture of M multivariate Gaussian distributions. Given $x \in \mathcal{X}$, for each mixture component $m \in [M]$, the hypernetwork outputs the logit $z_m(x)$ (for the categorical distribution over the mixture components), the mean $\mu_m(x)$ (component location), and the lower triangular Cholesky factor $L_m(x)$ (representing the scale of the covariance matrix).

The mixture weights $\pi_m(x)$ are obtained by applying the softmax function to the logits $z_m(x)$, ensuring they sum to 1. The covariance matrices $\Sigma_m(x)$ for each component are constructed by taking the product $L_m(x)L_m(x)^\top$, guaranteeing that they are positive semi-definite.

The density function evaluated in $y \in \mathcal{Y}$ conditional to $x \in \mathcal{X}$ is given by:

$$\hat{f}(y | x) = \sum_{m=1}^M \pi_m(x) \cdot \mathcal{N}(y | \mu_m(x), \Sigma_m(x)).$$

The model is trained using maximum likelihood estimation with $M = 10$.

Similarly to Distributional Random Forests, this method does not operate in a latent space, and thus we do not consider **L-CP**. CD diagrams for this predictor are presented in Appendix C.2.

A.3 Metrics

Marginal coverage. Marginal coverage is measured using

$$\text{MC} = \frac{1}{|\mathcal{D}_{\text{test}}|} \sum_{(x,y) \in \mathcal{D}_{\text{test}}} \mathbb{1}(y \in \hat{R}(x)).$$

Region size. We report the mean region size

$$\text{Size} = \frac{1}{|\mathcal{D}_{\text{test}}|} \sum_{(x,y) \in \mathcal{D}_{\text{test}}} |\hat{R}(x)|.$$

To avoid large regions disproportionately affecting the result, we also report the logarithm of the geometric mean of the region size

$$\text{G. Size} = \frac{1}{|\mathcal{D}_{\text{test}}|} \sum_{(x,y) \in \mathcal{D}_{\text{test}}} \max\{\log |\hat{R}(x)|, \epsilon\},$$

where $\epsilon = 10^{-50}$ prevents issues where $|\hat{R}(x)| = 0$.

Computing the size of the region is challenging in high dimensions. Hence, we propose an unbiased estimator of the region size using importance sampling:

$$|\hat{C}(x)| = \int_{\mathcal{Y}} \mathbb{1}(y \in \hat{C}(x)) dy = \mathbb{E}_{\hat{Y} \sim \hat{f}(x)} \left[\frac{\mathbb{1}(\hat{Y} \in \hat{C}(x))}{\hat{f}(\hat{Y} | x)} \right] \approx \frac{1}{K} \sum_{k=1}^K \frac{\mathbb{1}(\hat{Y}^{(k)} \in \hat{C}(x))}{\hat{f}(\hat{Y}^{(k)} | x)}, \quad (18)$$

where $\hat{Y}^{(k)} \sim \hat{f}(\cdot | x)$, $k \in [K]$. This estimator is compatible with all base predictors in Appendix A.2 since it is both possible to sample from their predictive distribution and evaluate the probability density function. In Appendix K of the supplementary material, we discuss the efficiency of this estimator.

Conditional coverage. To ensure a robust evaluation of conditional coverage, we consider three different conditional coverage metrics, detailed in Appendix A.5. The Worst Slab Coverage (WSC, Cauchois et al., 2021) groups inputs into "slabs" and evaluates the worst obtained coverage. The coverage error conditional to X (CEC-X) partitions the input space \mathcal{X} and evaluates coverage on each subset. The coverage error conditional to $V = \hat{f}(\hat{Y} | X)$, where $\hat{Y} \sim \hat{f}(\cdot | X)$, (CEC-V, Izbicki et al., 2022; Dheur et al., 2024), creates a partition based on the distribution of V , which is more robust to high-dimensional inputs.

A.4 Multi-Model, Multi-Dataset Comparison

In order to determine whether there are significant differences in model performance, we first apply the Friedman test (Friedman, 1940). Following the recommendations of Benavoli et al. (2016), we then conduct a pairwise post-hoc analysis using the Wilcoxon signed-rank test (Wilcoxon, 1945), coupled with Holm's alpha correction (Holm, 1979) to adjust for multiple comparisons.

The results are visualized using critical difference (CD) diagrams (Demšar, 2006). In these diagrams, models are ranked, with a lower rank (positioned further to the right) indicating better performance. A thick horizontal line connects models whose performances are not statistically different at the 0.05 significance level.

For MC and WSC, the CD diagrams report $|\text{MC} - (1 - \alpha)|$ and $|\text{WSC} - (1 - \alpha)|$, both of which should be minimized.

A.5 Metrics of Conditional Coverage

Worst Slab Coverage. Introduced in Cauchois et al., 2021, the *Worst Slab Coverage* (WSC) metric quantifies the minimal coverage over all possible slabs in \mathbb{R}^d , where each slab contains at least a fraction δ of the total mass, with $0 < \delta \leq 1$. For a given vector $v \in \mathbb{R}^d$, the WSC associated with v , denoted as WSC_v , is defined by:

$$\text{WSC}_v = \inf_{a < b} \left\{ \hat{\mathbb{P}}_{\mathcal{D}_{\text{test}}} \left(y_i \in \hat{R}(x_i) \mid a \leq v^\top x_i \leq b \right) \text{ s.t. } \hat{\mathbb{P}}_{\mathcal{D}_{\text{test}}} (a \leq v^\top x_i \leq b) \geq \delta \right\}, \quad (19)$$

where $a, b \in \mathbb{R}$. This metric assesses conditional coverage by focusing on inputs x_i that lie within a slab defined by v , using the inner product $v^\top x_i$ to measure similarity.

To estimate the worst-case slab, we follow the method from Cauchois et al., 2021, uniformly sampling 1,000 vectors v_j from the unit sphere \mathbb{S}^{d-1} and calculating:

$$\text{WSC} = \min_{v_j \in \mathbb{S}^{d-1}} \text{WSC}_{v_j}. \quad (20)$$

To mitigate overfitting on the test dataset, we partition the test set into two subsets, $\mathcal{D}_{\text{test}} = \mathcal{D}_{\text{test}}^{(1)} \cup \mathcal{D}_{\text{test}}^{(2)}$, as in Romano et al., 2020; Sesia and Romano, 2021. We identify the worst combination of a , b , and v on $\mathcal{D}_{\text{test}}^{(1)}$ by minimizing the WSC metric with $\delta = 0.2$, and then evaluate conditional coverage on the separate subset $\mathcal{D}_{\text{test}}^{(2)}$.

CEC-X. CEC-X approximates conditional coverage by partitioning the input space $X \in \mathcal{X} \subseteq \mathbb{R}^p$. We apply the k -means++ clustering algorithm on the inputs $X^{(i)}$ in the validation dataset \mathcal{D}_{val} , creating a partition $\mathcal{A} = A_1 \cup \dots \cup A_J$ over \mathcal{X} . The *Coverage Error Conditional to X* is defined as:

$$\text{CEC-X} = \frac{1}{|\mathcal{D}_{\text{test}}|} \sum_{i=1}^{|\mathcal{D}_{\text{test}}|} \sum_{j=1}^J \left(\hat{\mathbb{P}}_{\mathcal{D}_{\text{test}}} \left(y^{(i)} \in \hat{R}(x^{(i)}) \mid x^{(i)} \in A_j \right) - (1 - \alpha) \right)^2. \quad (21)$$

CEC-V. CEC-V is similar to CEC-X, but the conditioning is on the distribution of $\log V = \log \hat{f}(\hat{Y} | X)$, where $\hat{Y} \sim \hat{f}(\cdot | X)$. Unlike CEC-X, CEC-V is more robust to high-dimensional inputs. This approach originates from the CD-split⁺ method (Izbicki et al., 2022) and has been adapted to multivariate outputs in Dheur et al., 2024.

In practice, given an input x , a new feature v_x is created. First, samples v_i from $V | X = x$ are generated by sampling $y_1, \dots, y_m \sim \hat{f}(\cdot | x)$ and evaluating $v_i = \hat{f}(y_i | x)$. The resulting vector $v_x = (v_{(1)}, \dots, v_{(m)})$ consists of the order statistics $v_{(i)}$ from v_1, \dots, v_m .

The k -means++ clustering algorithm is applied on the vectors $\log v_{X^{(i)}}$ in the validation dataset \mathcal{D}_{val} , and a partition $\mathcal{A}_V = A_1 \cup \dots \cup A_J$ over \mathbb{R}^m is obtained. The *Coverage Error Conditional to the distribution of V* is then computed according to (21), using the partition \mathcal{A}_V .

Dheur et al., 2024 notes that the distance function corresponding to this partitioning approach is the 2-Wasserstein distance with respect to the distribution of V .

B Additional illustrative examples

B.1 Toy examples

We define two simple data-generating processes to evaluate the models compared to a known distribution: a unimodal heteroscedastic distribution and a bimodal heteroscedastic distribution. The input variable $X \in \mathbb{R}$ is unidimensional ($p = 1$) and the output variable $Y \in \mathbb{R}^2$ is bidimensional ($d = 2$). The variables X and Y are scaled linearly such that the mean and variances on each dimension are 0 and 1. The figures are inspired by Barrio et al., 2022.

Unimodal heteroscedastic process The first process is illustrated in Figure 2 in the main text. The data generating process is as follows:

$$X \sim \mathcal{U}(0.5, 2), \quad (22)$$

$$Y | X = x \sim \mathcal{N}(0, xI_d), \quad (23)$$

where I_d is a $d \times d$ identity matrix.

Bimodal heteroscedastic process Figure 5, similar to Figure 2 but with a bimodal distribution for the output, is introduced in Section 4.1.

The data generating process is as follows:

$$X \sim \mathcal{U}(0.5, 2), \quad (24)$$

$$Y | X = x \sim 0.5 \cdot \mathcal{N}(4, xI_d) + 0.5 \cdot \mathcal{N}(-4, I_d/x). \quad (25)$$

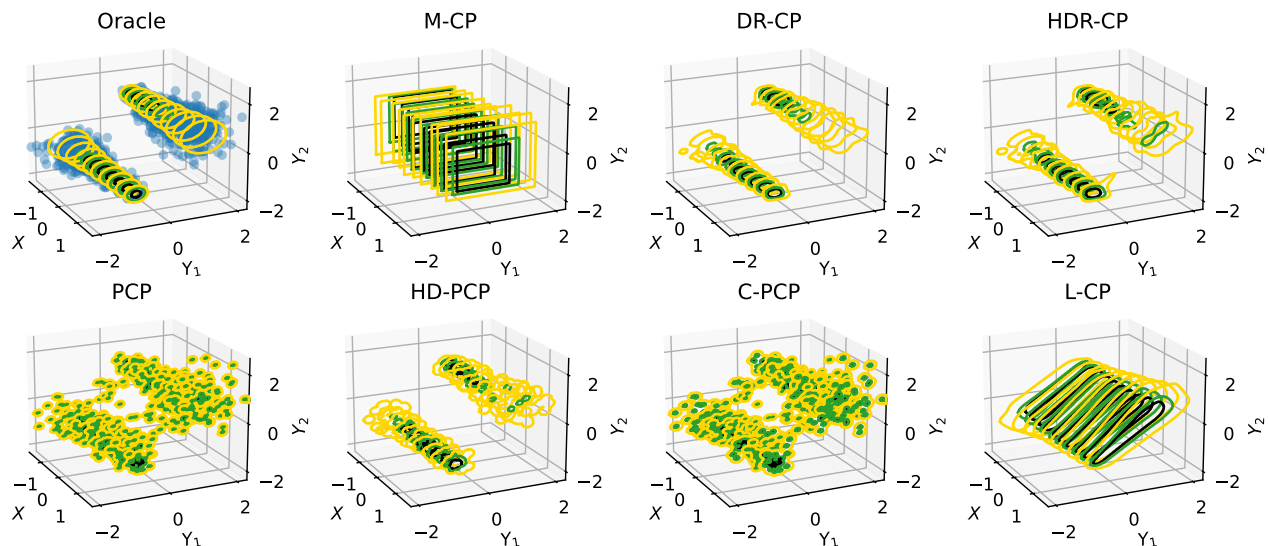


Figure 5: Examples of prediction regions on a bivariate bimodal dataset, conditional on a unidimensional input.

B.2 A real-world application

Following Wang et al., 2023a, we apply the multi-output conformal methods to the taxi dataset, where the goal is to predict the drop-off location of a New York taxi passenger based on the passenger’s information.

Panel 6(a) displays five randomly selected samples from the dataset, showing the pick-up (red pin) and drop-off (blue pin) locations of taxi passengers. The remaining panels show a specific input-output pair (x, y) and the corresponding prediction regions generated by the conformal methods discussed in this paper. The coverage level $1 - \alpha$ for these regions is set to 0.8, with MQF^2 as the base predictor, as introduced in Section A.2. Each region is labeled with its size, calculated using the estimator from Section A.3, displayed in the bottom left corner. Notably, C-PCP generates regions similar in shape to PCP but with an input-adaptive radius, resulting in smaller region sizes (8.2 compared to 8.67) in this case. Additionally, HD-PCP produces more clustered regions, while PCP and C-PCP show more dispersed regions.

Figure 7 presents the same example for an input-output pair where the input is associated with higher uncertainty, resulting in larger region sizes. As in the first figure, the shapes of the regions (e.g., unions of hyperrectangles, quantile regions, etc.) remain consistent but expand to cover a larger area. The order of the region sizes differs between the two figures, with HDR-CP producing the smallest region in the first figure and DR-CP in the second. In this case, C-PCP selects a larger radius than PCP, resulting in larger regions than PCP. The observation that PCP and C-PCP produce more dispersed regions, while HD-PCP generates more clustered regions, also holds true for this higher uncertainty case.

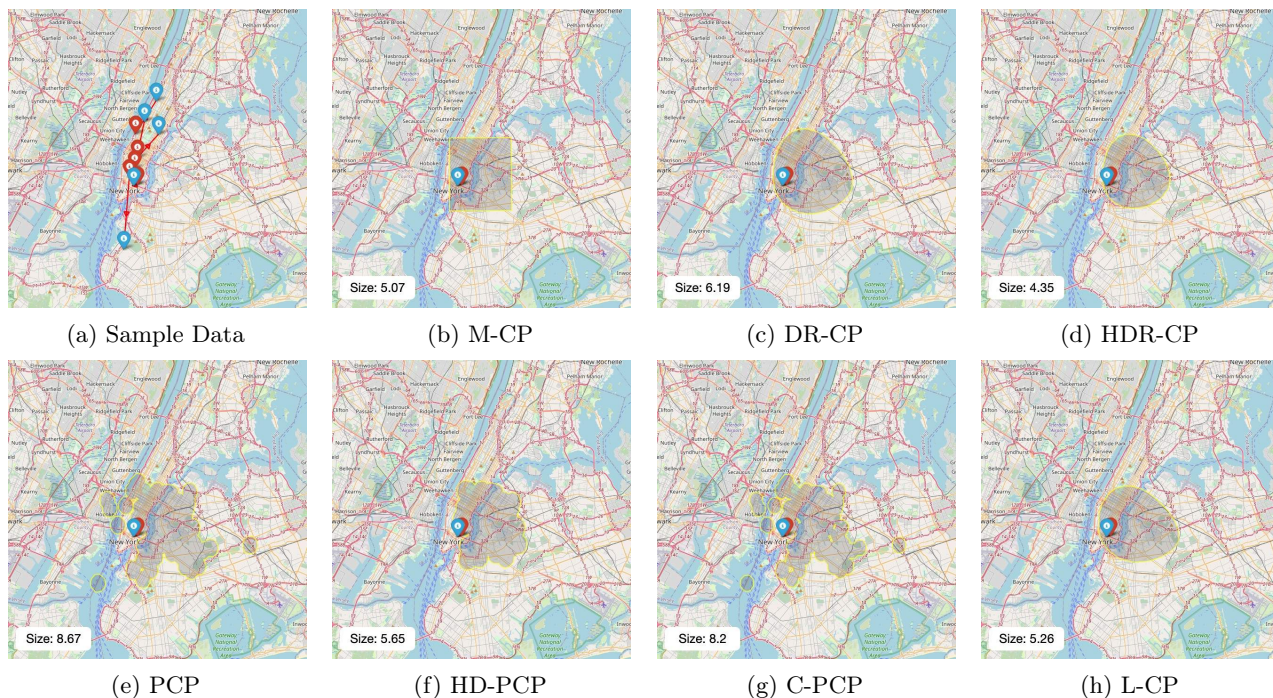


Figure 6: Conformal methods applied on the NYC Taxi dataset for an input with low uncertainty.

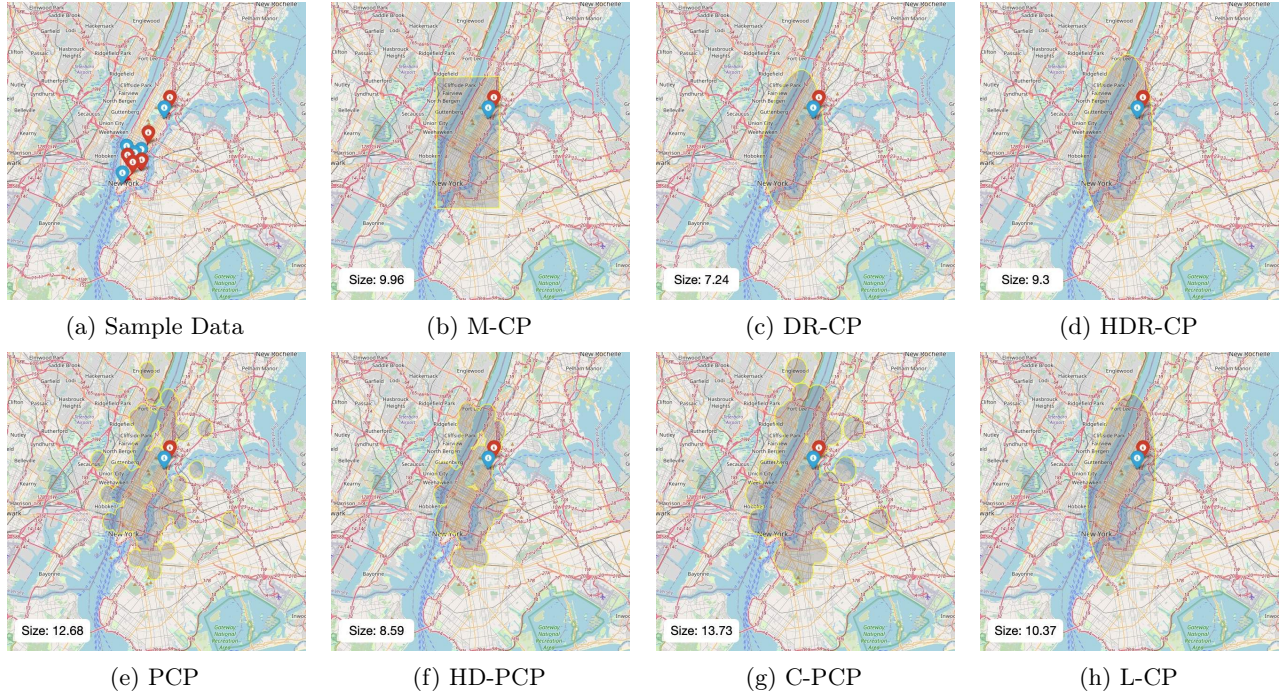


Figure 7: Conformal methods applied on the NYC Taxi dataset for an input with high uncertainty.

C Additional results

C.1 Distributional Random Forests

Figure 8 shows CD diagrams obtained with Distributional Random Forests as the base predictor. The experimental setup is described in Appendix A. Compared to the CD diagrams for MQF^2 (Figure 4), the results are very similar.

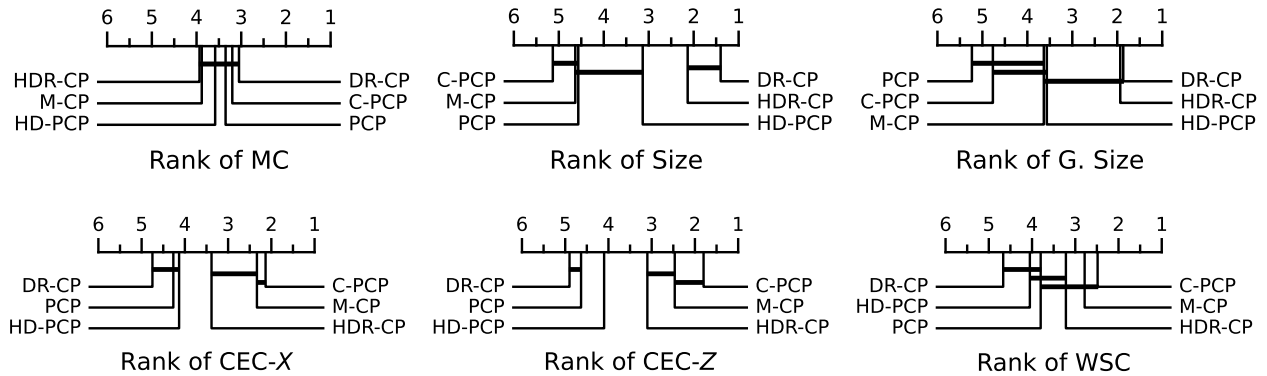


Figure 8: CD diagrams with the base predictor Distributional Random Forests based on 10 runs per dataset and method.

C.2 Multivariate Gaussian Mixture Model parameterized by a hypernetwork

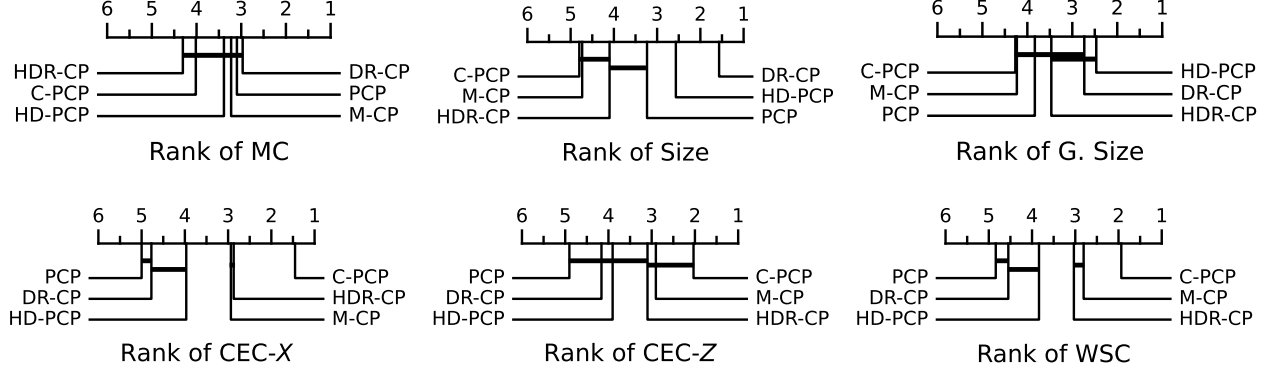


Figure 9: CD diagrams based on Multivariate Gaussian Mixture Model parameterized by a hypernetwork with $M = 10$ and 10 runs per dataset and method.

D Proofs

D.1 Distribution of the marginal coverage conditional on calibration data

In contrast to M-CP, L-CP, and DR-CP, the methods HDR-CP, PCP, HD-PCP, and C-PCP rely on a non-deterministic conformity score. For each calibration and test point, HDR-CP, PCP, HD-PCP, and C-PCP require sampling K , L , L , and $L + K$ points, respectively.

Let $\mathcal{D}_{\text{cal}} = \{(X^{(j)}, Y^{(j)})\}_{j \in [|\mathcal{D}_{\text{cal}}|]}$ represent the calibration dataset and (X, Y) be the test instance. Let $\mathcal{S}_{\text{cal}} = \{\mathcal{S}_{\text{cal}}^{(j)}\}_{j \in [|\mathcal{D}_{\text{cal}}|]}$ represent samples from the calibration dataset where $\mathcal{S}_{\text{cal}}^{(j)}$ is generated based on input $X^{(j)}$ and $\mathcal{S}_{\text{test}}$ the samples generated based on input X . Despite the added sampling uncertainty, these methods still provide a marginal coverage guarantee:

$$\mathbb{P}_{X, Y, \mathcal{S}_{\text{test}}, \mathcal{D}_{\text{cal}}, \mathcal{S}_{\text{cal}}}(Y \in \hat{R}(X)) \geq 1 - \alpha. \quad (26)$$

Compared to (3), the probability is additionally on \mathcal{S}_{cal} and $\mathcal{S}_{\text{test}}$. This result, specifically for PCP and HD-PCP, was demonstrated by Wang et al., 2023b.

In Lemma 1, we further show that the marginal coverage conditional on the calibration dataset \mathcal{D}_{cal} and the samples \mathcal{S}_{cal} follows a beta distribution, using standard arguments. Assuming no ties among the scores, this lemma applies to any conformity score s .

Lemma 1. Assuming no ties among the scores and i.i.d. inputs, outputs and samples, the distribution of the coverage, conditional on the calibration dataset and its samples, is given by:

$$\mathbb{P}(Y \in \hat{R}(X) \mid \mathcal{D}_{\text{cal}}, \mathcal{S}_{\text{cal}}) \sim \text{Beta}(k_{\alpha}, |\mathcal{D}_{\text{cal}}| + 1 - k_{\alpha}), \quad (27)$$

where $k_{\alpha} = \lceil (1 - \alpha)(|\mathcal{D}_{\text{cal}}| + 1) \rceil$. Moreover, $\mathbb{P}(Y \in \hat{R}(X)) = \frac{k_{\alpha}}{|\mathcal{D}_{\text{cal}}| + 1} \geq 1 - \alpha$.

Proof. For the methods HDR-CP, PCP, HD-PCP, and C-PCP, the conformity score s is non-deterministic due to sampling uncertainty. To clarify, we define a deterministic conformity score $\bar{s} : \mathcal{X} \times \mathcal{Y} \times \mathbb{S}$, where \mathbb{S} represents the space of samples for a given method.

For $j = 1, \dots, |\mathcal{D}_{\text{cal}}|$, let $S_j = \bar{s}(X^{(j)}, Y^{(j)}, \mathcal{S}_{\text{cal}}^{(j)})$ denote the conformity score on the calibration dataset, and let $S = \bar{s}(X, Y, \mathcal{S}_{\text{test}})$ represent the conformity score for the test instance. Since \bar{s} is deterministic and the tuples $(X^{(1)}, Y^{(1)}, \mathcal{S}_{\text{cal}}^{(1)}), \dots, (X^{(|\mathcal{D}_{\text{cal}}|)}, Y^{(|\mathcal{D}_{\text{cal}}|)}, \mathcal{S}_{\text{cal}}^{(|\mathcal{D}_{\text{cal}}|)})$, $(X, Y, \mathcal{S}_{\text{test}})$ are i.i.d. random variables, $S_1, \dots, S_{|\mathcal{D}_{\text{cal}}|}, S$ are also i.i.d. random variables.

Since $S_1, \dots, S_{|\mathcal{D}_{\text{cal}}|}, S$ are identically distributed, they share the same CDF. Using the probability integral transform, $F_S(S) \sim U(0, 1)$. Thus, $F_S(S_1), \dots, F_S(S_{|\mathcal{D}_{\text{cal}}|})$ correspond to uniform variates $U_1, \dots, U_{|\mathcal{D}_{\text{cal}}|}$. Since there are no ties among the scores, F_S is strictly increasing, and $F_S(S_{(j)}) = U_{(j)}$ for $j = 1, \dots, |\mathcal{D}_{\text{cal}}|$, where $S_{(j)}$ and $U_{(j)}$ are the j -th order statistics. Hence:

$$\mathbb{P}(Y \in \hat{R}(X) \mid \mathcal{D}_{\text{cal}}, \mathcal{S}_{\text{cal}}) = \mathbb{P}(S \leq S_{(k_\alpha)} \mid S_1, \dots, S_{|\mathcal{D}_{\text{cal}}|}) \quad (28)$$

$$= F_S(S_{(k_\alpha)}) \quad (29)$$

$$= U_{(k_\alpha)} \quad (30)$$

$$\sim \text{Beta}(k_\alpha, |\mathcal{D}_{\text{cal}}| + 1 - k_\alpha). \quad (31)$$

The final step results from the distribution of uniform order statistics. Taking the expectation of the Beta distribution gives:

$$\mathbb{P}(Y \in \hat{R}(X)) = \mathbb{E}[\mathbb{P}(Y \in \hat{R}(X) \mid \mathcal{D}_{\text{cal}}, \mathcal{S}_{\text{cal}})] = \frac{k_\alpha}{|\mathcal{D}_{\text{cal}}| + 1} \geq 1 - \alpha. \quad (32)$$

□

D.2 Proofs of asymptotic conditional coverage

D.2.1 L-CP

Proposition 2. Assuming $|\mathcal{D}_{\text{cal}}| \rightarrow \infty$ and $\hat{Q}(Z; X) \stackrel{\text{d}}{=} Y|X$, L-CP achieves asymptotic conditional coverage.

Proof. We first show that the conditional coverage of L-CP is equal to the CDF of the random variable $d_{\mathcal{Z}}(Z)$ in \hat{q} , i.e., $F_{d_{\mathcal{Z}}(Z)}(\hat{q})$. Given $x \in \mathcal{X}$, we have:

$$\mathbb{P}(Y \in \hat{R}_{\text{L-CP}}(X) \mid X = x) \quad (33)$$

$$= \mathbb{P}(Y \in \{\hat{Q}(z; x) : z \in R_{\mathcal{Z}}(\hat{q})\} \mid X = x) \quad (34)$$

$$= \mathbb{P}(\hat{Q}^{-1}(Y; X) \in R_{\mathcal{Z}}(\hat{q}) \mid X = x) \quad (\text{Invertibility of } \hat{Q}(\cdot; X)) \quad (35)$$

$$= \mathbb{P}(Z \in R_{\mathcal{Z}}(\hat{q})) \quad (\hat{Q}(Z; X) \stackrel{\text{d}}{=} Y|X) \quad (36)$$

$$= \mathbb{P}(d_{\mathcal{Z}}(Z) \leq \hat{q}) \quad (37)$$

$$= F_{d_{\mathcal{Z}}(Z)}(\hat{q}). \quad (38)$$

Marginalizing over X , we obtain that the marginal coverage is also equal to $F_{d_{\mathcal{Z}}(Z)}(\hat{q})$:

$$\mathbb{P}(Y \in \hat{R}_{\text{L-CP}}(X)) \quad (39)$$

$$= \mathbb{E}_X \left[\mathbb{P}(Y \in \hat{R}_{\text{L-CP}}(X) \mid X) \right] \quad (40)$$

$$= \mathbb{E}_X [F_{d_{\mathcal{Z}}(Z)}(\hat{q})] \quad (41)$$

$$= F_{d_{\mathcal{Z}}(Z)}(\hat{q}) \quad (42)$$

In the limit of $|\mathcal{D}_{\text{cal}}| \rightarrow \infty$, thanks to the Glivenko-Cantelli theorem, $\mathbb{P}(Y \in \hat{R}_{\text{L-CP}}(X)) = 1 - \alpha$ and the quantile \hat{q} obtained by SCP is thus $F_{d_{\mathcal{Z}}(Z)}^{-1}(1 - \alpha)$.

Finally, we obtain that the conditional coverage is equal to $1 - \alpha$:

$$\mathbb{P}(Y \in \hat{R}_{\text{L-CP}}(X) \mid X = x) \quad (43)$$

$$= F_{d_{\mathcal{Z}}(Z)}(F_{d_{\mathcal{Z}}(Z)}^{-1}(1 - \alpha)) \quad (44)$$

$$= 1 - \alpha. \quad (45)$$

□

D.2.2 HDR-CP and C-PCP

Lemma 2. Assuming $|D_{\text{cal}}| \rightarrow \infty$, any conformal method with conformity score s_{CDF} (14) achieves asymptotic conditional coverage, independently from the conformity score s_W of the base method. With the additional assumption that $K \rightarrow \infty$ and $\hat{f} = f$, s_{ECDF} (15) achieves asymptotic conditional coverage.

Proof. Let $W = s_W(X, Y)$ and consider $x \in \mathcal{X}$ and $y \in \mathcal{Y}$. By the probability integral transform, $s_{\text{CDF}}(x, Y) = F_{W|X=x}(W | X = x) \sim \mathcal{U}(0, 1)$.

Marginalizing over X , we obtain:

$$\mathbb{P}(Y \in \hat{R}_{\text{CDF}}(X)) = \mathbb{P}(s_{\text{CDF}}(X, Y) \leq \hat{q}) \tag{46}$$

$$= \mathbb{E}_X[\mathbb{P}(s_{\text{CDF}}(X, Y) \leq \hat{q} | X)] \tag{47}$$

$$= \mathbb{E}_X[\mathbb{P}(U \leq \hat{q})] \tag{48}$$

$$= \mathbb{E}_X[\hat{q}] \tag{49}$$

$$= \hat{q}, \tag{50}$$

where $U \sim \mathcal{U}(0, 1)$. In the limit of $|D_{\text{cal}}| \rightarrow \infty$, thanks to the Glivenko-Cantelli theorem, $\mathbb{P}(Y \in \hat{R}_{\text{CDF}}(X)) = 1 - \alpha$ and the quantile \hat{q} obtained by SCP is thus $1 - \alpha$.

Finally, we note that:

$$\mathbb{P}(Y \in \hat{R}_{\text{CDF}}(X) | X = x) = \mathbb{P}(s_{\text{CDF}}(X, Y) \leq \hat{q} | X = x) \tag{51}$$

$$= \mathbb{P}(U \leq 1 - \alpha) \tag{52}$$

$$= 1 - \alpha. \tag{53}$$

Assuming $\hat{f} = f$, observe that, for any $x \in \mathcal{X}$ and $y \in \mathcal{Y}$, $s_{\text{ECDF}}(x, y) \rightarrow s_{\text{CDF}}(x, y)$ as $K \rightarrow \infty$ by the law of large numbers. Thus, under these conditions, any conformal method with conformity score s_{ECDF} achieves conditional coverage. □

Proposition 3. Assuming $|D_{\text{cal}}| \rightarrow \infty$ and $K \rightarrow \infty$, both HDR-CP and C-PCP with the oracle base predictor $\hat{f} = f$ achieve conditional coverage.

Proof. The proof is direct by Lemma 2 with $s_W(x, y) = s_{\text{DR-CP}}(x, y)$ for HDR-CP and $s_W(x, y) = s_{\text{PCP}}(x, y)$ for C-PCP. □

D.2.3 M-CP

Consider M-CP with exact quantile estimates $\hat{l}_i(x) = Q_{Y_i}(\alpha_l | x)$ and $\hat{u}_i(x) = Q_{Y_i}(\alpha_u | x)$ where $Q_{Y_i}(\alpha | x)$ is the quantile function of Y_i conditional to $X = x$ evaluated in α . This section introduces two propositions where M-CP requests two different nominal coverage levels $\alpha_u - \alpha_l$, namely $\sqrt[d]{1 - \alpha}$ and $1 - \alpha$. The propositions show that M-CP can achieve conditional coverage under two contrasting scenarios: independence or total dependence between the dimensions of the output.

Proposition 4. Assuming Y_1, \dots, Y_d are conditionally independent given X , M-CP achieves conditional coverage if $\alpha_u - \alpha_l = \sqrt[d]{1 - \alpha}$.

Proof. For any $x \in \mathcal{X}$ and $i \in [d]$, we first establish that the $\sqrt[d]{1 - \alpha}$ th quantile of the distribution of $s_i(X, Y_i)$

given $X = x$ equals 0:

$$\mathbb{P}(s_i(X, Y_i) \leq 0 \mid X = x) = \mathbb{P}(\max\{l_i(X) - Y, Y - u_i(X)\} \leq 0 \mid X = x) \quad (54)$$

$$= \mathbb{P}(l_i(X) \leq Y \wedge Y \leq u_i(X) \mid X = x) \quad (55)$$

$$= 1 - \mathbb{P}(l_i(X) > Y \vee Y > u_i(X) \mid X = x) \quad (56)$$

$$= 1 - \mathbb{P}(l_i(X) > Y \mid X = x) - \mathbb{P}(Y > u_i(X) \mid X = x) \quad (57)$$

$$= 1 - \alpha_l - (1 - \alpha_u) \quad (58)$$

$$= \alpha_u - \alpha_l \quad (59)$$

$$= \sqrt[d]{1 - \alpha}. \quad (60)$$

Using (60), we show that the $1 - \alpha$ th quantile of the distribution of $s(X, Y)$ given $X = x$ is 0:

$$\mathbb{P}(s_{\text{M-CP}}(X, Y) \leq 0 \mid X = x) = \mathbb{P}(s_i(X, Y_i) \leq 0, \forall i \in [d] \mid X = x) \quad (61)$$

$$= \mathbb{P}(s_1(X, Y_1) \leq 0 \wedge \dots \wedge s_d(X, Y_d) \leq 0 \mid X = x) \quad (62)$$

$$= \mathbb{P}(s_1(X, Y_1) \leq 0 \mid X = x) \dots \mathbb{P}(s_d(X, Y_d) \leq 0 \mid X = x) \quad (63)$$

$$= \sqrt[d]{1 - \alpha}^d \quad (64)$$

$$= 1 - \alpha, \quad (65)$$

where (63) is obtained by conditional independence of Y_1, \dots, Y_d given X . Marginalizing over X , we obtain that the $1 - \alpha$ th quantile of $s(X, Y)$ is 0:

$$\mathbb{P}(s_{\text{M-CP}}(X, Y) \leq 0) = \mathbb{E}_X[\mathbb{P}(s_{\text{M-CP}}(X, Y) \leq 0 \mid X)] \quad (66)$$

$$= \mathbb{E}_X[1 - \alpha] \quad (67)$$

$$= 1 - \alpha. \quad (68)$$

In the limit of $|\mathcal{D}_{\text{cal}}| \rightarrow \infty$, thanks to the Glivenko-Cantelli theorem, $\mathbb{P}(Y \in \hat{R}_{\text{M-CP}}(X)) = 1 - \alpha$ and the quantile \hat{q} obtained by SCP is thus 0.

Finally, using (65) and $\hat{q} = 0$, we obtain that **M-CP** achieves conditional coverage:

$$\mathbb{P}(Y \in \hat{R}_{\text{M-CP}}(X) \mid X = x) = \mathbb{P}(s_{\text{M-CP}}(X, Y) \leq \hat{q} \mid X = x) = 1 - \alpha. \quad (69)$$

□

Proposition 5. Assuming $Y_1|X \stackrel{\text{a.s.}}{=} \dots \stackrel{\text{a.s.}}{=} Y_d|X$, **M-CP** achieves conditional coverage if $\alpha_u - \alpha_l = 1 - \alpha$.

Proof. Let $x \in \mathcal{X}$. Using (59), we first show that the $1 - \alpha$ th conditional quantile of the distribution of $s_i(X, Y_i)$, for any $i \in [d]$, is 0:

$$\mathbb{P}(s_i(X, Y_i) \leq 0 \mid X = x) = \alpha_u - \alpha_l \quad (70)$$

$$= 1 - \alpha. \quad (71)$$

Using (71), we show that the $1 - \alpha$ th quantile of the distribution of $s(X, Y)$ given X is 0:

$$\mathbb{P}(s(X, Y) \leq 0 \mid X = x) = \mathbb{P}(s_i(X, Y_i) \leq 0, \forall i \in [d] \mid X = x) \quad (72)$$

$$= \mathbb{P}(s_1(X, Y_1) \leq 0 \wedge \dots \wedge s_d(X, Y_d) \leq 0 \mid X = x) \quad (73)$$

$$= \mathbb{P}(s_1(X, Y_1) \leq 0 \mid X = x) \quad (74)$$

$$= 1 - \alpha, \quad (75)$$

where (74) is due to $Y_1|X \stackrel{\text{a.s.}}{=} \dots \stackrel{\text{a.s.}}{=} Y_d|X$, which implies that, conditional to $X = x$, $l_1(X) = \dots = l_d(X)$ and $u_1(X) = \dots = u_d(X)$ and thus $s_1(X, Y_1) = \dots = s_d(X, Y_d)$. Using (68), we obtain that $\hat{q} = 0$. Finally, using (75), we obtain that **M-CP** achieves conditional coverage:

$$\mathbb{P}(Y \in \hat{R}(X) \mid X = x) = \mathbb{P}(s(X, Y) \leq 0 \mid X = x) = 1 - \alpha. \quad (76)$$

□

D.3 Connection between sample-based and density-based methods

This section proves the connections between sample-based and density-based methods as introduced in Section 4.3. We start by restating a known lemma of conformal prediction.

Lemma 3. Consider a conformal prediction method with conformity score s . If $g : \mathbb{R} \rightarrow \mathbb{R}$ is a strictly increasing function, then the method with conformity score $g \circ s$ will produce the same prediction regions.

Proof. For any $x \in \mathcal{X}$, consider the prediction region created with s as in Section 2.1:

$$\hat{R}(x) = \{y \in \mathcal{Y} : s(x, y) \leq \text{Quantile}(\{s_i\}_{i \in [D_{\text{cal}}]} \cup \{\infty\}; k_\alpha)\}. \quad (77)$$

Since g is strictly increasing,

$$\hat{R}(x) = \{y \in \mathcal{Y} : g(s(x, y)) \leq g(\text{Quantile}(\{s_i\}_{i \in [D_{\text{cal}}]} \cup \{\infty\}; k_\alpha))\} \quad (78)$$

$$= \{y \in \mathcal{Y} : g(s(x, y)) \leq \text{Quantile}(\{g(s_i)\}_{i \in [D_{\text{cal}}]} \cup \{\infty\}; k_\alpha)\}. \quad (79)$$

Since (79) corresponds to the prediction region with conformity score $g \circ s$, this shows that the two methods create the same regions. \square

Proposition 1. PCP is equivalent to DR-CP with $\hat{f} = \hat{f}_{\max}$. Similarly, HD-PCP is equivalent to DR-CP with $\hat{f} = \hat{f}_{\max}$ where only $\lfloor (1 - \alpha)L \rfloor$ samples with the highest density among $\{\tilde{Y}^{(l)}\}_{l \in [L]}$ are kept. Finally, C-PCP is equivalent to HDR-CP with $\hat{f} = \hat{f}_{\max}$.

Proof. In the following proof, we note $a \uparrow b$ to signify that there exists a strictly increasing function g such that $a = g(b)$. Consider DR-CP with $\hat{f} = \hat{f}_{\max}$. We have:

$$s_{\text{DR-CP}}(x, y) = -\hat{f}_{\max}(y | x) \quad (80)$$

$$\uparrow -\max_{l \in [L]} f_{\mathbb{S}}(y; \tilde{Y}^{(l)}) \quad \left(\hat{f}_{\max}(y | x) = \max_{l \in [L]} f_{\mathbb{S}}(y; \tilde{Y}^{(l)})/C \right) \quad (81)$$

$$= \min_{l \in [L]} -f_{\mathbb{S}}(y; \tilde{Y}^{(l)}) \quad (82)$$

$$\uparrow \min_{l \in [L]} \|y - \tilde{Y}^{(l)}\|_2 \quad (f_{\mathbb{S}}(y; \tilde{Y}^{(l)}) \text{ has spherical level sets centered at } \tilde{Y}^{(l)}) \quad (83)$$

$$= s_{\text{PCP}}(x, y). \quad (84)$$

We obtain the equivalence between the two methods by Lemma 3. The proof for HD-PCP follows the same arguments.

We now consider HDR-CP with $\hat{f} = \hat{f}_{\max}$. We have:

$$s_{\text{HDR-CP}}(x, y) = \frac{1}{K} \sum_{k \in [K]} \mathbb{1}(\hat{f}_{\max}(\hat{Y}^{(k)} | x) \geq \hat{f}_{\max}(y | x)) \quad \text{where } \hat{Y}^{(k)} \sim \hat{f}(\cdot | x), k \in [K]. \quad (85)$$

Developing the inequality for $k \in [K]$, we obtain:

$$\hat{f}_{\max}(\hat{Y}^{(k)} | x) \geq \hat{f}_{\max}(y | x) \quad (86)$$

$$\iff \max_{l \in [L]} f_{\mathbb{S}}(\hat{Y}^{(k)}; \hat{Y}^{(l)}) \geq \max_{l \in [L]} f_{\mathbb{S}}(y; \hat{Y}^{(l)}) \quad \left(\hat{f}_{\max}(y | x) = \max_{l \in [L]} f_{\mathbb{S}}(y; \tilde{Y}^{(l)})/C \right) \quad (87)$$

$$\iff \min_{l \in [L]} -f_{\mathbb{S}}(\hat{Y}^{(k)}; \hat{Y}^{(l)}) \leq \min_{l \in [L]} -f_{\mathbb{S}}(y; \hat{Y}^{(l)}) \quad (88)$$

$$\iff \min_{l \in [L]} \|\hat{Y}^{(k)} - \hat{Y}^{(l)}\|_2 \leq \min_{l \in [L]} \|y - \tilde{Y}^{(l)}\|_2. \quad (f_{\mathbb{S}}(y; \tilde{Y}^{(l)}) \text{ has spherical level sets centered at } \tilde{Y}^{(l)}) \quad (89)$$

$$(90)$$

Noting that (85) with (90) corresponds to the conformity score of C-PCP, we obtain the equivalence. \square

E Results on an image dataset

To better understand the behavior of prediction regions in high-dimensional spaces, we apply conformal methods to the CIFAR-10 dataset (Krizhevsky et al., 2014), which consists of 32x32 RGB images, each labeled with one of 10 possible classes. We train a generative model conditioned on the image label, where $\mathcal{Y} = [0, 1]^{3 \times 32 \times 32}$ ($d = 3072$) represents the image space, and $\mathcal{X} = \{0, \dots, 9\}$ ($p = 1$) represents the labels. The training, calibration, and test datasets contain 50,000, 1,500, and 1,500 images, respectively. As noted in Angelopoulos and Bates, 2021, this calibration dataset size is sufficient to ensure good marginal coverage.

Our generative model is a conditional Glow model (Kingma and Dhariwal, 2018) based on the implementation from Stimper et al., 2022 using a 3-level multi-scale architecture with 32 blocks per level. Like MQF² (Appendix A.2), this generative model is a normalizing flow and directly compatible with all methods presented, except M-CP. For a direct comparison with M-CP, we compute quantiles based on samples from the generative model as in Appendix A.2.

The latent space of the conditional Glow model, due to its multi-scale architecture, consists of three subspaces: $\mathcal{Z} = \mathcal{Z}_1 \times \mathcal{Z}_2 \times \mathcal{Z}_3$, where $\mathcal{Z}_1 = \mathbb{R}^{48 \times 4 \times 4}$, $\mathcal{Z}_2 = \mathbb{R}^{12 \times 8 \times 8}$, and $\mathcal{Z}_3 = \mathbb{R}^{6 \times 16 \times 16}$. As the distance function $d_{\mathcal{Z}}$ in the latent space, we use the maximum norm across the three spaces to penalize high norms in any of them: $d_{\mathcal{Z}}(z) = \max\{\|z_1\|_2, \|z_2\|_2, \|z_3\|_2\}$, where $z = z_1 \times z_2 \times z_3$.

Table 2 presents the metrics introduced in Appendix A.3. All methods achieve marginal coverage despite the high dimensionality of \mathcal{Y} , which is expected as the marginal coverage distribution conditional on the calibration dataset is independent of d (Appendix D.1). Despite using the logarithm of the geometric mean, we observe that the G. Size metric has a high magnitude. DR-CP achieves the smallest G. Size, closely followed by HDR-CP. The mean region size is not reported because it diminishes to zero, as machine precision cannot represent such small values.

Regarding conditional coverage, as in other experiments, L-CP, HDR-CP, C-PCP, and M-CP exhibit the smallest CEC- X and CEC- Z values, indicating superior conditional coverage. The WSC metric supports similar conclusions, with DR-CP and PCP being the least calibrated.

Dataset	Method	MC	G. Size	CEC- X	CEC- Z ($\times 100$)	WSC ($\times 100$)
CIFAR-10	M-CP	0.782	-7.47e+03	0.252	0.142	0.741
	DR-CP	0.787	-9.09e+03	0.516	0.451	0.730
	HDR-CP	0.794	-9.07e+03	0.280	0.0151	0.761
	PCP	0.791	-7.47e+03	0.476	0.305	0.736
	HD-PCP	0.791	-7.47e+03	0.523	0.293	0.780
	C-PCP	0.815	-7.45e+03	0.116	0.0642	0.792
	L-CP	0.806	-7.50e+03	0.0716	0.134	0.818

Table 2: Results obtained with a conditional Glow model on CIFAR-10 with $1 - \alpha = 0.8$.

F Datasets

Table 3 provides the characteristics of each dataset considered in this study.

Table 3: Characteristics of each dataset considered in this study.

Source	Dataset	Nb instances	Nb features p	Nb targets d
Mulan	slump	103	7	3
	edm	154	16	2
	atp7d	296	348	6
	sf1	323	31	3
	oes97	334	263	16
	atp1d	337	347	6
	jura	359	6	3
	oes10	403	298	16
	osales	556	19	12
	enb	768	2	2
Wang	energy	768	2	2
Mulan	wq	1060	16	14
	sf2	1066	31	3
	scpf	1137	4	3
Del Barrio	ansur2	1986	1	2
Camehl	households	7207	4	4
Mulan	scm20d	8966	60	16
	rf1	9005	64	8
	rf2	9005	64	8
	scm1d	9803	279	16
Cevid	wage	10000	4	2
	births2	10000	7	4
	births1	10000	6	2
	air	10000	5	6
Feldman	meps_21	15656	137	2
	meps_19	15785	137	2
	meps_20	17541	137	2
	house	21613	14	2
	bio	45730	8	2
	blog_data	50000	55	2
Del Barrio	calcofi	50000	1	2
Wang	taxi	50000	4	2

G Computation Time

Table 4 compares the total computation time for calculating the conformity scores on the calibration dataset and evaluating whether $Y \in \hat{R}(X)$ for each instance (X, Y) in the test dataset. Each metric is the mean over 10 independent runs. The standard error of the mean is indicated as an index.

L-CP is consistently the fastest, followed by DR-CP. However, M-CP, HDR-CP, C-PCP, and HD-PCP each require generating $K = 100$ or $L = 100$ samples for every instance in both the calibration and test datasets, which accounts for their longer runtime. C-PCP needs to generate $K + L = 200$ samples for each instance, resulting in the highest overall computation time.

Table 4: Total time, in seconds, to compute the scores over the calibration dataset and evaluating the marginal coverage over the test set.

Dataset	M-CP	DR-CP	HDR-CP	PCP	HD-PCP	C-PCP	L-CP
slump	0.188 _{0.050}	0.0113 _{0.0017}	0.206 _{0.053}	0.192 _{0.054}	0.203 _{0.057}	0.377 _{0.10}	0.00808 _{0.00028}
edm	0.445 _{0.13}	0.0102 _{0.0017}	0.459 _{0.13}	0.437 _{0.13}	0.445 _{0.13}	0.878 _{0.25}	0.00793 _{0.00014}
atp7d	0.290 _{0.073}	0.0318 _{0.011}	0.337 _{0.081}	0.268 _{0.063}	0.291 _{0.068}	0.552 _{0.13}	0.00945 _{8.2e-05}
sf1	0.696 _{0.23}	0.0166 _{0.0034}	0.719 _{0.24}	0.670 _{0.21}	0.684 _{0.21}	1.36 _{0.44}	0.00945 _{0.00017}
oes97	0.273 _{0.076}	0.0393 _{0.010}	0.355 _{0.092}	0.246 _{0.062}	0.297 _{0.074}	0.513 _{0.14}	0.00975 _{0.00018}
atp1d	0.239 _{0.056}	0.0333 _{0.012}	0.287 _{0.065}	0.261 _{0.066}	0.283 _{0.071}	0.492 _{0.12}	0.00995 _{0.00015}
jura	0.220 _{0.062}	0.0151 _{0.0028}	0.242 _{0.066}	0.199 _{0.053}	0.213 _{0.057}	0.412 _{0.12}	0.00997 _{0.00013}
oes10	0.281 _{0.070}	0.0432 _{0.012}	0.368 _{0.088}	0.300 _{0.077}	0.353 _{0.090}	0.574 _{0.15}	0.0106 _{0.00021}
osales	85.13.1e+01	0.0477 _{0.016}	85.23.1e+01	67.52.4e+01	67.52.4e+01	1.53e+02 _{5.3e+01}	0.0119 _{0.00045}
enb	0.239 _{0.057}	0.0210 _{0.0054}	0.255 _{0.060}	0.245 _{0.062}	0.252 _{0.064}	0.471 _{0.12}	0.0132 _{0.00016}
wq	1.92 _{0.66}	0.0532 _{0.011}	2.00 _{0.68}	1.92 _{0.67}	1.97 _{0.68}	3.82 _{1.3}	0.0190 _{0.00042}
sf2	1.69 _{0.62}	0.0507 _{0.021}	1.74 _{0.62}	1.72 _{0.63}	1.74 _{0.64}	3.39 _{1.3}	0.0188 _{0.00030}
scpf	2.15 _{0.65}	0.0340 _{0.0092}	2.19 _{0.65}	2.12 _{0.64}	2.14 _{0.64}	4.26 _{1.3}	0.0191 _{0.00029}
ansur2	0.582 _{0.16}	0.118 _{0.027}	0.689 _{0.17}	0.556 _{0.15}	0.580 _{0.16}	1.11 _{0.31}	0.0405 _{0.0042}
households	3.36 _{1.0}	0.679 _{0.20}	4.09 _{1.0}	2.07 _{0.42}	2.19 _{0.44}	5.34 _{1.4}	0.114 _{0.0032}
scm20d	2.33 _{0.52}	0.592 _{0.23}	3.17 _{0.74}	2.33 _{0.53}	2.65 _{0.59}	4.60 _{1.0}	0.119 _{0.0030}
rf2	5.66 _{1.5}	0.466 _{0.20}	6.25 _{1.6}	5.53 _{1.4}	5.71 _{1.5}	11.1 _{2.9}	0.113 _{0.0014}
rfl	5.48 _{1.4}	0.471 _{0.20}	6.06 _{1.5}	5.56 _{1.5}	5.74 _{1.5}	11.0 _{2.9}	0.114 _{0.0015}
scm1d	2.34 _{0.55}	0.767 _{0.35}	3.39 _{0.90}	2.33 _{0.54}	2.69 _{0.62}	4.62 _{1.1}	0.117 _{0.0013}
births2	1.11e+02 _{3.3e+01}	1.11 _{0.35}	1.12e+02 _{3.3e+01}	1.15e+02 _{3.7e+01}	1.15e+02 _{3.7e+01}	2.26e+02 _{7.0e+01}	0.134 _{0.0076}
air	10.23.8	1.05 _{0.32}	11.43.8	8.32 _{3.0}	8.57 _{3.0}	18.46.7	0.134 _{0.0057}
births1	32.01.2e+01	1.07 _{0.35}	33.11.2e+01	33.21.2e+01	33.31.2e+01	65.12.4e+01	0.137 _{0.0091}
wage	41.31.4e+01	1.18 _{0.38}	42.51.4e+01	41.11.4e+01	41.21.4e+01	82.32.9e+01	0.142 _{0.0088}
meps_21	35.61.0e+01	0.844 _{0.49}	36.51.0e+01	35.11.0e+01	35.21.0e+01	70.62.0e+01	0.137 _{0.0018}
meps_19	49.21.7e+01	0.852 _{0.49}	50.11.7e+01	51.41.8e+01	51.51.8e+01	1.00e+02 _{3.4e+01}	0.145 _{0.0081}
meps_20	42.71.3e+01	1.01 _{0.60}	43.71.3e+01	42.31.2e+01	42.41.2e+01	84.92.5e+01	0.144 _{0.0024}
house	13.34.2	1.07 _{0.62}	14.44.3	12.73.9	12.83.9	25.98.1	0.167 _{0.0016}
bio	55.91.6e+01	8.38 _{3.0}	65.11.6e+01	60.91.9e+01	61.81.9e+01	1.17e+02 _{3.4e+01}	0.280 _{0.022}
blog_data	2.63e+02 _{7.6e+01}	4.67 _{3.0}	2.68e+02 _{7.6e+01}	2.60e+02 _{7.5e+01}	2.61e+02 _{7.5e+01}	5.23e+02 _{1.5e+02}	0.270 _{0.0028}
calcofi	21.54.5	11.24.1	33.78.5	23.45.0	24.55.2	44.89.4	0.303 _{0.010}
taxi	13.73.8	0.278 _{0.038}	14.13.9	13.63.8	13.93.9	27.27.6	0.263 _{0.0039}

H Full results

Tables 5 to 8 show the full results obtained with the setup described in Section 6. Each metric is the mean over 10 independent runs. The standard error of the mean is indicated as an index.

Table 5: Full results obtained with the setup described in Section 6 (Part 1).

Dataset	Method	MC	G. Size	Size	CEC-X ($\times 100$)	CEC-Z ($\times 100$)	WSC
slump	M-CP	0.841 _{0.029}	1.76 _{0.36}	18.4 _{7.4}	3.56 _{0.55}	6.12 _{1.2}	1.00 _{0.0}
	DR-CP	0.786 _{0.039}	1.92 _{0.35}	20.4 _{7.6}	6.45 _{2.5}	8.55 _{1.7}	0.947 _{0.037}
	HDR-CP	0.945 _{0.039}	2.29 _{0.45}	1.45e+02 _{7.4e+01}	4.67 _{0.41}	5.73 _{0.83}	0.983 _{0.017}
	PCP	0.836 _{0.034}	1.71 _{0.36}	17.9 _{8.9}	4.10 _{0.87}	5.39 _{1.2}	0.975 _{0.025}
	HD-PCP	0.818 _{0.033}	1.63 _{0.35}	16.7 _{8.6}	4.10 _{0.89}	5.34 _{1.2}	0.982 _{0.018}
	C-PCP	0.891 _{0.030}	1.92 _{0.36}	27.5 _{9.3}	3.95 _{0.55}	4.97 _{0.66}	1.00 _{0.0}
	L-CP	0.818 _{0.033}	2.15 _{0.41}	35.7 _{1.0e+01}	6.74 _{1.9}	8.78 _{1.8}	0.930 _{0.052}
edm	M-CP	0.756 _{0.030}	-0.607 _{0.38}	2.38 _{0.51}	4.36 _{0.67}	3.55 _{0.44}	0.704 _{0.080}
	DR-CP	0.800 _{0.024}	-0.444 _{0.38}	3.04 _{1.2}	4.67 _{0.66}	3.24 _{0.53}	0.797 _{0.041}
	HDR-CP	0.869 _{0.045}	-0.578 _{0.38}	4.06 _{1.3}	3.77 _{0.26}	3.50 _{0.45}	0.777 _{0.10}
	PCP	0.775 _{0.029}	-0.438 _{0.41}	3.29 _{0.94}	4.57 _{0.71}	3.66 _{0.49}	0.782 _{0.088}
	HD-PCP	0.762 _{0.034}	-0.556 _{0.42}	2.43 _{0.57}	4.61 _{0.81}	3.64 _{0.49}	0.832 _{0.075}
	C-PCP	0.803 _{0.041}	-0.523 _{0.39}	3.58 _{1.1}	4.50 _{0.68}	3.43 _{0.54}	0.792 _{0.082}
	L-CP	0.781 _{0.024}	-0.553 _{0.35}	3.23 _{1.1}	4.87 _{0.78}	3.00 _{0.59}	0.849 _{0.060}
atp7d	M-CP	0.841 _{0.016}	2.02 _{0.24}	3.76e+02 _{9.6e+01}	4.21 _{0.53}	1.47 _{0.18}	0.796 _{0.060}
	DR-CP	0.807 _{0.011}	2.43 _{0.17}	5.73e+02 _{1.8e+02}	4.76 _{1.4}	3.40 _{1.0}	0.808 _{0.061}
	HDR-CP	0.918 _{0.042}	3.39 _{0.20}	1.67e+04 _{6.1e+03}	4.09 _{0.055}	5.33 _{0.74}	0.906 _{0.067}
	PCP	0.808 _{0.020}	2.06 _{0.19}	2.04e+02 _{4.6e+01}	5.77 _{1.4}	4.32 _{0.90}	0.771 _{0.074}
	HD-PCP	0.813 _{0.018}	1.96 _{0.19}	1.68e+02 _{3.6e+01}	6.01 _{1.3}	4.04 _{1.0}	0.711 _{0.093}
	C-PCP	0.839 _{0.020}	2.76 _{0.17}	3.79e+03 _{4.6e+02}	3.04 _{0.42}	2.92 _{0.46}	0.904 _{0.034}
	L-CP	0.805 _{0.020}	3.15 _{0.17}	5.21e+03 _{7.0e+02}	3.37 _{0.50}	5.46 _{1.3}	0.835 _{0.070}
sfl	M-CP	0.839 _{0.0096}	-2.79 _{0.86}	14.2 _{6.8}	4.32 _{1.4}	2.21 _{0.34}	0.875 _{0.054}
	DR-CP	0.847 _{0.012}	-2.32 _{0.76}	9.20 _{3.8}	4.37 _{0.91}	2.82 _{0.46}	0.872 _{0.031}
	HDR-CP	0.847 _{0.013}	-4.11 _{0.94}	12.5 _{4.6}	3.94 _{0.88}	1.68 _{0.27}	0.875 _{0.039}
	PCP	0.841 _{0.014}	-2.11 _{0.72}	14.5 _{4.2}	4.25 _{0.87}	3.06 _{0.63}	0.832 _{0.061}
	HD-PCP	0.833 _{0.013}	-2.31 _{0.71}	9.71 _{2.4}	4.22 _{0.86}	3.07 _{0.61}	0.820 _{0.037}
	C-PCP	0.835 _{0.013}	-3.39 _{0.86}	19.7 _{5.0}	3.52 _{0.83}	1.64 _{0.22}	0.884 _{0.037}
	L-CP	0.841 _{0.011}	-3.94 _{0.91}	12.0 _{3.9}	3.83 _{0.92}	1.77 _{0.29}	0.875 _{0.043}
oes97	M-CP	0.809 _{0.022}	1.81 _{0.98}	8.03e+06 _{4.3e+06}	5.06 _{0.76}	2.89 _{0.51}	0.716 _{0.060}
	DR-CP	0.804 _{0.022}	-2.10 _{2.4}	1.39e+07 _{9.8e+06}	5.56 _{0.76}	4.48 _{0.85}	0.599 _{0.098}
	HDR-CP	0.956 _{0.029}	5.96 _{1.1}	7.38e+10 _{2.8e+10}	3.61 _{0.36}	3.74 _{0.26}	0.960 _{0.040}
	PCP	0.799 _{0.026}	-5.30 _{2.8}	1.21e+07 _{1.1e+07}	9.30 _{1.3}	10.9 _{1.6}	0.443 _{0.086}
	HD-PCP	0.797 _{0.027}	-5.35 _{2.8}	1.11e+07 _{1.0e+07}	9.28 _{1.3}	10.8 _{1.6}	0.418 _{0.12}
	C-PCP	0.809 _{0.016}	3.24 _{1.0}	1.31e+09 _{4.2e+08}	2.88 _{0.68}	2.25 _{0.39}	0.755 _{0.091}
	L-CP	0.816 _{0.022}	5.75 _{1.1}	2.07e+10 _{5.9e+09}	2.39 _{0.47}	3.22 _{0.73}	0.915 _{0.032}
atp1d	M-CP	0.797 _{0.019}	0.0495 _{0.21}	70.7 _{8.2}	2.57 _{0.59}	1.86 _{0.39}	0.758 _{0.097}
	DR-CP	0.825 _{0.016}	0.713 _{0.29}	1.19e+02 _{3.0e+01}	2.34 _{0.62}	2.36 _{0.44}	0.856 _{0.049}
	HDR-CP	0.916 _{0.028}	1.60 _{0.22}	4.88e+03 _{1.9e+03}	2.76 _{0.46}	3.60 _{0.24}	0.924 _{0.040}
	PCP	0.793 _{0.018}	0.386 _{0.25}	33.5 _{8.4}	6.76 _{0.97}	7.97 _{0.93}	0.502 _{0.11}
	HD-PCP	0.794 _{0.018}	0.271 _{0.24}	25.8 _{5.5}	6.80 _{1.0}	7.82 _{1.0}	0.579 _{0.12}
	C-PCP	0.823 _{0.020}	0.739 _{0.26}	1.39e+03 _{2.9e+02}	1.61 _{0.19}	2.77 _{0.56}	0.739 _{0.065}
	L-CP	0.813 _{0.014}	1.31 _{0.22}	2.13e+03 _{3.7e+02}	1.53 _{0.15}	3.10 _{0.68}	0.793 _{0.053}
jura	M-CP	0.808 _{0.021}	6.46e+14 _{6.5e+14}	∞	2.89 _{0.53}	1.30 _{0.14}	0.740 _{0.046}
	DR-CP	0.801 _{0.021}	1.36 _{0.15}	8.20 _{1.6}	2.81 _{0.57}	1.50 _{0.25}	0.787 _{0.055}
	HDR-CP	0.808 _{0.031}	5.51e+13 _{5.5e+13}	∞	3.28 _{0.48}	2.19 _{0.43}	0.795 _{0.053}
	PCP	0.796 _{0.020}	6.46e+14 _{6.5e+14}	∞	3.18 _{0.70}	1.57 _{0.24}	0.721 _{0.064}
	HD-PCP	0.815 _{0.019}	6.46e+14 _{6.5e+14}	∞	2.73 _{0.55}	1.46 _{0.21}	0.853 _{0.043}
	C-PCP	0.795 _{0.028}	6.46e+14 _{6.5e+14}	∞	2.98 _{0.47}	2.00 _{0.44}	0.824 _{0.044}
	L-CP	0.805 _{0.028}	1.46 _{0.17}	12.2 _{1.3}	2.78 _{0.45}	2.11 _{0.28}	0.815 _{0.065}
oes10	M-CP	0.807 _{0.014}	0.798 _{1.0}	2.91e+06 _{1.0e+06}	3.67 _{0.53}	1.25 _{0.19}	0.808 _{0.040}
	DR-CP	0.830 _{0.013}	-3.65 _{2.1}	1.02e+06 _{1.0e+06}	5.05 _{0.54}	3.12 _{0.47}	0.671 _{0.063}
	HDR-CP	0.974 _{0.026}	4.96 _{1.1}	3.78e+10 _{7.9e+09}	4.12 _{0.024}	3.83 _{0.17}	0.988 _{0.012}
	PCP	0.818 _{0.018}	-5.66 _{1.7}	1.22e+05 _{4.7e+04}	8.61 _{0.64}	9.46 _{1.1}	0.421 _{0.050}
	HD-PCP	0.818 _{0.018}	-5.67 _{1.7}	1.21e+05 _{4.7e+04}	8.61 _{0.64}	9.46 _{1.1}	0.502 _{0.12}
	C-PCP	0.824 _{0.014}	2.31 _{1.0}	1.48e+09 _{3.9e+08}	2.28 _{0.31}	1.83 _{0.48}	0.798 _{0.048}
	L-CP	0.800 _{0.018}	4.53 _{1.1}	2.53e+10 _{7.8e+09}	2.01 _{0.34}	3.54 _{0.77}	0.827 _{0.048}
osales	M-CP	0.796 _{0.014}	9.28e+22 _{9.3e+22}	∞	2.68 _{0.44}	3.97 _{0.72}	0.578 _{0.098}
	DR-CP	0.779 _{0.017}	6.48 _{1.7}	6.64e+12 _{6.6e+12}	3.06 _{0.39}	4.24 _{0.68}	0.543 _{0.090}
	HDR-CP	0.823 _{0.032}	7.34e+18 _{5.7e+18}	∞	3.17 _{0.47}	4.11 _{0.70}	0.706 _{0.061}
	PCP	0.785 _{0.016}	9.09e+18 _{5.6e+18}	∞	2.74 _{0.45}	3.93 _{0.71}	0.556 _{0.078}
	HD-PCP	0.786 _{0.016}	9.08e+18 _{5.6e+18}	∞	2.73 _{0.45}	3.92 _{0.71}	0.578 _{0.11}
	C-PCP	0.830 _{0.031}	9.05e+18 _{5.6e+18}	∞	3.15 _{0.49}	4.12 _{0.70}	0.617 _{0.10}
	L-CP	0.778 _{0.017}	6.07 _{1.9}	6.64e+12 _{6.6e+12}	3.06 _{0.39}	4.22 _{0.68}	0.504 _{0.11}

Multi-Output Conformal Regression

Table 6: Full results obtained with the setup described in Section 6 (Part 2).

Dataset	Method	MC	G. Size	Size	CEC-X ($\times 100$)	CEC-Z ($\times 100$)	WSC
enb	M-CP	0.823 _{0.013}	-0.803 _{0.074}	0.815 _{0.073}	1.16 _{0.16}	1.12 _{0.15}	0.781 _{0.032}
	DR-CP	0.812 _{0.0094}	-1.15 _{0.079}	0.389_{0.039}	2.45 _{0.48}	2.33 _{0.35}	0.615 _{0.063}
	HDR-CP	0.810 _{0.011}	-1.31_{0.078}	0.540 _{0.047}	1.05 _{0.19}	0.877 _{0.16}	0.724 _{0.049}
	PCP	0.806 _{0.012}	-0.810 _{0.082}	0.596 _{0.058}	2.53 _{0.30}	3.00 _{0.44}	0.624 _{0.042}
	HD-PCP	0.815 _{0.0096}	-0.969 _{0.068}	0.518 _{0.038}	1.77 _{0.27}	2.04 _{0.26}	0.696 _{0.028}
	C-PCP	0.803_{0.0090}	-0.999 _{0.074}	0.744 _{0.066}	0.627_{0.092}	0.616_{0.11}	0.785_{0.026}
	L-CP	0.814 _{0.015}	-1.14 _{0.073}	0.639 _{0.039}	0.949 _{0.18}	0.810 _{0.14}	0.784 _{0.024}
wq	M-CP	0.810_{0.0076}	13.6 _{2.1}	1.40e+10 _{5.2e+09}	0.511_{0.10}	0.415_{0.096}	0.799_{0.028}
	DR-CP	0.811 _{0.012}	12.6 _{1.8}	1.91e+08_{8.2e+07}	2.10 _{0.56}	0.690 _{0.20}	0.771 _{0.038}
	HDR-CP	0.930 _{0.030}	13.7 _{1.6}	2.12e+11 _{1.9e+11}	2.95 _{0.49}	2.78 _{0.50}	0.913 _{0.036}
	PCP	0.814 _{0.012}	12.7 _{1.9}	6.65e+08 _{2.8e+08}	0.976 _{0.21}	0.826 _{0.14}	0.791 _{0.028}
	HD-PCP	0.814 _{0.012}	12.6_{1.9}	5.46e+08 _{2.3e+08}	0.727 _{0.11}	0.734 _{0.10}	0.803 _{0.025}
	C-PCP	0.815 _{0.012}	12.9 _{1.9}	6.08e+09 _{3.8e+09}	1.05 _{0.26}	0.811 _{0.12}	0.791 _{0.025}
	L-CP	0.817 _{0.0082}	13.4 _{1.6}	9.28e+09 _{4.0e+09}	2.36 _{0.47}	0.802 _{0.15}	0.782 _{0.038}
sf2	M-CP	0.816 _{0.011}	-8.40 _{0.91}	2.60 _{0.60}	3.05 _{0.78}	1.71 _{0.32}	0.727 _{0.045}
	DR-CP	0.825 _{0.0071}	-8.78 _{0.97}	0.267_{0.12}	4.20 _{0.53}	4.10 _{1.0}	0.581 _{0.056}
	HDR-CP	0.857 _{0.025}	-8.90_{0.65}	2.87 _{1.4}	2.42 _{0.34}	2.17 _{0.38}	0.843_{0.043}
	PCP	0.827 _{0.0091}	-7.21 _{1.2}	1.77 _{0.73}	3.07 _{0.45}	3.26 _{0.62}	0.712 _{0.038}
	HD-PCP	0.821 _{0.010}	-7.30 _{1.2}	1.82 _{0.66}	2.89 _{0.42}	2.83 _{0.54}	0.711 _{0.045}
	C-PCP	0.822 _{0.014}	-8.14 _{0.98}	23.5 _{1.7e+01}	2.24_{0.45}	1.38_{0.28}	0.755 _{0.046}
	L-CP	0.815_{0.0083}	-8.64 _{0.65}	2.93 _{0.96}	2.74 _{0.42}	1.59 _{0.32}	0.638 _{0.065}
scpf	M-CP	0.808 _{0.0084}	-7.30 _{0.58}	2.72 _{0.65}	3.18 _{0.43}	2.82 _{0.46}	0.709 _{0.031}
	DR-CP	0.806 _{0.010}	-9.61_{0.79}	0.217_{0.15}	8.51 _{0.85}	8.35 _{1.0}	0.400 _{0.079}
	HDR-CP	0.802_{0.011}	-8.53 _{0.66}	2.53 _{0.54}	1.97 _{0.30}	1.47 _{0.24}	0.715 _{0.041}
	PCP	0.807 _{0.013}	-6.95 _{0.81}	0.980 _{0.75}	7.13 _{0.75}	7.13 _{0.78}	0.506 _{0.071}
	HD-PCP	0.805 _{0.013}	-6.88 _{0.73}	0.754 _{0.56}	6.92 _{0.73}	6.86 _{0.76}	0.514 _{0.060}
	C-PCP	0.804 _{0.011}	-7.40 _{0.60}	6.42 _{1.3}	1.43_{0.25}	1.15_{0.23}	0.787_{0.031}
	L-CP	0.806 _{0.0059}	-8.43 _{0.64}	3.00 _{0.56}	3.19 _{0.36}	2.82 _{0.40}	0.747 _{0.040}
ansur2	M-CP	0.792 _{0.0078}	1.32 _{0.021}	3.81 _{0.080}	0.196_{0.051}	0.422 _{0.095}	0.778 _{0.014}
	DR-CP	0.788 _{0.0069}	1.20_{0.018}	3.34_{0.058}	0.270 _{0.054}	0.496 _{0.14}	0.777 _{0.020}
	HDR-CP	0.798_{0.0096}	1.23 _{0.019}	3.49 _{0.064}	0.326 _{0.073}	0.507 _{0.14}	0.757 _{0.019}
	PCP	0.776 _{0.0092}	1.51 _{0.014}	4.64 _{0.066}	0.380 _{0.068}	0.508 _{0.14}	0.773 _{0.019}
	HD-PCP	0.785 _{0.0076}	1.27 _{0.014}	3.59 _{0.050}	0.258 _{0.045}	0.446 _{0.079}	0.772 _{0.012}
	C-PCP	0.788 _{0.0085}	1.54 _{0.016}	4.83 _{0.078}	0.309 _{0.050}	0.357_{0.068}	0.798_{0.017}
	L-CP	0.795 _{0.0065}	1.21 _{0.015}	3.36 _{0.050}	0.264 _{0.047}	0.412 _{0.10}	0.749 _{0.018}
households	M-CP	0.798 _{0.0047}	2.57 _{0.035}	34.8 _{1.5}	0.334 _{0.061}	0.354 _{0.041}	0.784 _{0.010}
	DR-CP	0.801 _{0.0049}	2.36 _{0.029}	13.6_{0.45}	1.07 _{0.10}	2.36 _{0.17}	0.646 _{0.014}
	HDR-CP	0.806 _{0.0035}	2.19_{0.023}	36.3 _{1.3}	0.177 _{0.041}	0.101 _{0.027}	0.809_{0.0071}
	PCP	0.799 _{0.0045}	2.86 _{0.027}	31.6 _{1.3}	1.03 _{0.099}	2.33 _{0.11}	0.650 _{0.019}
	HD-PCP	0.799_{0.0046}	2.59 _{0.030}	27.0 _{1.6}	0.762 _{0.099}	1.55 _{0.098}	0.673 _{0.014}
	C-PCP	0.804 _{0.0033}	2.65 _{0.030}	63.8 _{2.4}	0.135_{0.040}	0.0714_{0.019}	0.810 _{0.0039}
	L-CP	0.804 _{0.0043}	2.69 _{0.030}	54.0 _{1.6}	0.214 _{0.046}	0.0922 _{0.017}	0.789 _{0.014}
scm20d	M-CP	0.800_{0.0045}	5.28 _{0.13}	6.18e+07 _{2.1e+07}	0.0811_{0.019}	0.684 _{0.065}	0.765 _{0.012}
	DR-CP	0.797 _{0.0036}	4.09_{0.075}	1.11e+03_{7.3e+01}	0.510 _{0.048}	3.37 _{0.12}	0.681 _{0.014}
	HDR-CP	0.806 _{0.0036}	4.19 _{0.11}	2.94e+09 _{7.9e+08}	0.0923 _{0.016}	0.0645_{0.012}	0.800_{0.0092}
	PCP	0.794 _{0.0040}	4.15 _{0.13}	2.13e+04 _{2.4e+03}	0.563 _{0.068}	4.91 _{0.21}	0.634 _{0.016}
	HD-PCP	0.796 _{0.0039}	4.18 _{0.11}	2.41e+04 _{3.1e+03}	0.481 _{0.068}	4.39 _{0.21}	0.660 _{0.018}
	C-PCP	0.800_{0.0052}	4.64 _{0.13}	2.64e+09 _{7.8e+08}	0.172 _{0.031}	0.141 _{0.026}	0.776 _{0.012}
	L-CP	0.798 _{0.0041}	4.93 _{0.10}	2.89e+09 _{6.6e+08}	0.106 _{0.023}	0.0699 _{0.012}	0.786 _{0.0060}
rf2	M-CP	0.799_{0.0043}	-5.97 _{0.94}	∞	0.211 _{0.034}	0.886 _{0.14}	0.645 _{0.017}
	DR-CP	0.805 _{0.0038}	-9.31_{0.73}	0.0102_{0.0039}	1.03 _{0.22}	5.74 _{0.63}	0.517 _{0.041}
	HDR-CP	0.805 _{0.0036}	-7.62 _{0.93}	∞	0.0992 _{0.023}	0.226 _{0.064}	0.726_{0.015}
	PCP	0.806 _{0.0035}	-6.57 _{0.89}	∞	1.14 _{0.23}	5.90 _{0.44}	0.502 _{0.036}
	HD-PCP	0.806 _{0.0035}	-6.60 _{0.89}	∞	1.04 _{0.21}	5.50 _{0.43}	0.529 _{0.028}
	C-PCP	0.806 _{0.0040}	-6.46 _{0.95}	∞	0.0940_{0.020}	0.192_{0.048}	0.712 _{0.013}
	L-CP	0.804 _{0.0046}	-7.43 _{0.96}	2.86 _{1.2}	0.103 _{0.029}	0.207 _{0.050}	0.709 _{0.013}
rf1	M-CP	0.798_{0.0046}	-5.99 _{0.94}	∞	0.202 _{0.037}	0.891 _{0.14}	0.650 _{0.018}
	DR-CP	0.805 _{0.0036}	-9.34_{0.75}	0.0102_{0.0039}	1.03 _{0.21}	5.84 _{0.64}	0.519 _{0.039}
	HDR-CP	0.803 _{0.0035}	-7.50 _{0.89}	∞	0.0840_{0.022}	0.222 _{0.065}	0.726_{0.016}
	PCP	0.807 _{0.0036}	-6.61 _{0.89}	∞	1.13 _{0.23}	5.98 _{0.47}	0.506 _{0.036}
	HD-PCP	0.807 _{0.0037}	-6.65 _{0.90}	∞	1.04 _{0.21}	5.61 _{0.46}	0.532 _{0.030}
	C-PCP	0.806 _{0.0039}	-6.51 _{0.97}	∞	0.0932 _{0.020}	0.194_{0.048}	0.713 _{0.014}
	L-CP	0.803 _{0.0046}	-7.45 _{0.97}	2.87 _{1.2}	0.0894 _{0.025}	0.212 _{0.048}	0.713 _{0.015}

Table 7: Full results obtained with the setup described in Section 6 (Part 3).

Dataset	Method	MC	G. Size	Size	CEC-X ($\times 100$)	CEC-Z ($\times 100$)	WSC
scm1d	M-CP	0.797 _{0.0033}	0.620 _{0.087}	4.15e+05 _{9.0e+04}	0.920 _{0.078}	2.32 _{0.071}	0.625 _{0.013}
	DR-CP	0.794 _{0.0059}	-1.77_{0.15}	36.1_{4.5}	1.51 _{0.10}	5.50 _{0.18}	0.577 _{0.014}
	HDR-CP	0.806 _{0.0041}	-0.320 _{0.095}	9.23e+07 _{2.8e+07}	0.426_{0.046}	0.118_{0.012}	0.773_{0.018}
	PCP	0.797 _{0.0054}	-1.64 _{0.14}	3.28e+02 _{7.5e+01}	1.82 _{0.11}	8.06 _{0.23}	0.533 _{0.021}
	HD-PCP	0.798 _{0.0048}	-1.59 _{0.14}	3.79e+02 _{1.5e+02}	1.79 _{0.10}	7.86 _{0.21}	0.519 _{0.015}
	C-PCP	0.804 _{0.0039}	0.201 _{0.095}	1.29e+08 _{5.2e+07}	0.461 _{0.065}	0.144 _{0.013}	0.761 _{0.011}
	L-CP	0.802_{0.0036}	-0.313 _{0.080}	7.48e+07 _{3.0e+07}	0.431 _{0.044}	0.121 _{0.015}	0.751 _{0.0092}
births2	M-CP	0.799 _{0.0047}	6.35e+10 _{4.9e+10}	∞	0.331_{0.057}	0.113_{0.018}	0.701 _{0.020}
	DR-CP	0.801 _{0.0032}	1.86e+08_{1.7e+08}	∞	0.902 _{0.25}	0.531 _{0.27}	0.624 _{0.020}
	HDR-CP	0.837 _{0.028}	6.36e+10 _{4.9e+10}	∞	1.09 _{0.49}	0.943 _{0.51}	0.768_{0.042}
	PCP	0.812 _{0.012}	6.35e+10 _{4.9e+10}	∞	0.461 _{0.11}	0.502 _{0.22}	0.706 _{0.034}
	HD-PCP	0.811 _{0.011}	6.35e+10 _{4.9e+10}	∞	0.402 _{0.11}	0.327 _{0.15}	0.701 _{0.028}
	C-PCP	0.837 _{0.028}	6.36e+10 _{4.9e+10}	∞	1.04 _{0.50}	1.56 _{0.76}	0.757 _{0.048}
	L-CP	0.800_{0.0037}	1.86e+08 _{1.7e+08}	∞	0.817 _{0.27}	0.138 _{0.033}	0.644 _{0.032}
air	M-CP	0.798 _{0.0043}	4.92 _{0.050}	4.09e+02 _{2.5e+01}	0.0717_{0.015}	0.0910_{0.012}	0.787 _{0.0077}
	DR-CP	0.803 _{0.0039}	4.14 _{0.079}	71.24.8	0.102 _{0.018}	0.556 _{0.033}	0.785 _{0.011}
	HDR-CP	0.803 _{0.0052}	4.09_{0.096}	1.52e+02 _{1.0e+01}	0.141 _{0.025}	0.136 _{0.027}	0.797_{0.0081}
	PCP	0.800_{0.0043}	4.81 _{0.051}	2.05e+02 _{1.1e+01}	0.116 _{0.024}	0.809 _{0.044}	0.754 _{0.012}
	HD-PCP	0.801 _{0.0036}	4.64 _{0.047}	1.76e+02 _{1.1e+01}	0.109 _{0.026}	0.603 _{0.044}	0.781 _{0.012}
	C-PCP	0.803 _{0.0043}	4.81 _{0.049}	4.44e+02 _{2.2e+01}	0.0899 _{0.011}	0.106 _{0.020}	0.806 _{0.011}
	L-CP	0.799 _{0.0038}	5.22 _{0.048}	5.28e+02 _{2.2e+01}	0.154 _{0.018}	0.103 _{0.025}	0.776 _{0.011}
births1	M-CP	0.799 _{0.0030}	2.36 _{0.16}	17.1 _{3.0}	0.0661_{0.014}	0.0568_{0.013}	0.789_{0.0070}
	DR-CP	0.801_{0.0039}	-2.21_{0.63}	0.699_{0.47}	0.294 _{0.084}	0.856 _{0.27}	0.696 _{0.016}
	HDR-CP	0.806 _{0.0066}	-1.78 _{0.48}	1.49 _{0.47}	0.148 _{0.046}	0.405 _{0.092}	0.763 _{0.015}
	PCP	0.796 _{0.0033}	2.29 _{0.16}	17.1 _{3.3}	0.126 _{0.029}	0.246 _{0.066}	0.756 _{0.013}
	HD-PCP	0.794 _{0.0031}	2.28 _{0.17}	18.5 _{4.2}	0.104 _{0.023}	0.174 _{0.052}	0.771 _{0.0090}
	C-PCP	0.803 _{0.0037}	2.31 _{0.17}	19.3 _{4.0}	0.0915 _{0.019}	0.0935 _{0.019}	0.768 _{0.012}
	L-CP	0.793 _{0.0049}	2.25 _{0.16}	13.2 _{2.5}	0.115 _{0.021}	0.136 _{0.044}	0.774 _{0.011}
wage	M-CP	0.800_{0.0040}	20.8 _{8.1}	∞	0.0586 _{0.011}	0.261 _{0.047}	0.798_{0.0048}
	DR-CP	0.803 _{0.0049}	-2.12 _{0.14}	0.148_{0.019}	0.0791 _{0.013}	0.196 _{0.074}	0.773 _{0.020}
	HDR-CP	0.802 _{0.0049}	-2.14_{0.13}	0.217 _{0.026}	0.102 _{0.019}	0.833 _{0.19}	0.754 _{0.021}
	PCP	0.802 _{0.0040}	7.17 _{4.1}	∞	0.0466_{0.0095}	0.0767_{0.013}	0.797 _{0.010}
	HD-PCP	0.800 _{0.0043}	10.9 _{6.7}	∞	0.0540 _{0.0097}	0.200 _{0.046}	0.795 _{0.0063}
	C-PCP	0.808 _{0.0048}	4.39 _{3.0}	∞	0.0680 _{0.012}	0.454 _{0.058}	0.786 _{0.0097}
	L-CP	0.801 _{0.0049}	1.08 _{0.15}	9.64 _{1.9}	0.0839 _{0.013}	0.320 _{0.091}	0.768 _{0.012}
meps_21	M-CP	0.799 _{0.0026}	9.04 _{9.3}	∞	0.779 _{0.095}	0.646 _{0.13}	0.706 _{0.012}
	DR-CP	0.801 _{0.0010}	-3.11_{0.17}	0.257_{0.012}	3.90 _{0.18}	3.47 _{0.65}	0.520 _{0.012}
	HDR-CP	0.807 _{0.0036}	-3.05 _{0.16}	∞	0.580 _{0.22}	0.231 _{0.046}	0.739 _{0.027}
	PCP	0.800_{0.0023}	11.5 _{9.3}	∞	3.05 _{0.14}	2.94 _{0.56}	0.558 _{0.0071}
	HD-PCP	0.798 _{0.0022}	11.5 _{9.4}	∞	2.06 _{0.12}	1.70 _{0.33}	0.602 _{0.011}
	C-PCP	0.807 _{0.0030}	2.60 _{4.0}	∞	0.105_{0.034}	0.0695_{0.017}	0.794_{0.0068}
	L-CP	0.798 _{0.0034}	-2.70 _{0.23}	2.49 _{0.64}	1.04 _{0.44}	0.456 _{0.097}	0.700 _{0.029}
meps_19	M-CP	0.803 _{0.0033}	3.22e+14 _{3.2e+14}	∞	0.678 _{0.086}	0.507 _{0.15}	0.739 _{0.011}
	DR-CP	0.794 _{0.0025}	-3.70_{0.26}	0.222_{0.014}	4.04 _{0.17}	2.82 _{0.81}	0.504 _{0.014}
	HDR-CP	0.801 _{0.0063}	2.67e+14 _{2.7e+14}	∞	0.764 _{0.35}	0.284 _{0.17}	0.691 _{0.034}
	PCP	0.795 _{0.0039}	3.22e+14 _{3.2e+14}	∞	2.94 _{0.27}	3.30 _{1.0}	0.544 _{0.017}
	HD-PCP	0.799 _{0.0027}	3.22e+14 _{3.2e+14}	∞	2.01 _{0.19}	1.89 _{0.62}	0.600 _{0.010}
	C-PCP	0.801 _{0.0028}	3.22e+14 _{3.2e+14}	∞	0.188_{0.064}	0.218_{0.16}	0.788_{0.014}
	L-CP	0.800_{0.0040}	-2.67 _{0.17}	3.31 _{0.81}	1.39 _{0.52}	0.448 _{0.18}	0.646 _{0.045}
meps_20	M-CP	0.803_{0.0038}	-0.511 _{0.75}	∞	0.728 _{0.065}	0.525 _{0.12}	0.715 _{0.012}
	DR-CP	0.809 _{0.0038}	-2.98_{0.15}	0.306_{0.011}	3.37 _{0.16}	2.32 _{0.59}	0.548 _{0.012}
	HDR-CP	0.806 _{0.0032}	-2.97 _{0.12}	1.93e+09 _{1.9e+09}	0.290 _{0.041}	0.360 _{0.17}	0.744 _{0.023}
	PCP	0.805 _{0.0034}	12.1 _{6.0}	∞	2.81 _{0.088}	2.22 _{0.58}	0.559 _{0.0097}
	HD-PCP	0.805 _{0.0040}	19.6 _{9.2}	∞	1.87 _{0.088}	1.31 _{0.34}	0.612 _{0.013}
	C-PCP	0.808 _{0.0028}	3.08 _{2.5}	∞	0.0823_{0.015}	0.0677_{0.021}	0.788_{0.0055}
	L-CP	0.807 _{0.0019}	-2.56 _{0.17}	2.63 _{0.44}	0.653 _{0.23}	0.660 _{0.27}	0.697 _{0.032}
house	M-CP	0.802 _{0.0035}	0.104 _{0.022}	2.25 _{0.27}	0.169 _{0.015}	0.191 _{0.018}	0.759 _{0.0066}
	DR-CP	0.800_{0.0035}	-0.579_{0.028}	0.620_{0.017}	0.945 _{0.056}	1.61 _{0.10}	0.616 _{0.0070}
	HDR-CP	0.802 _{0.0046}	-0.569 _{0.025}	0.801 _{0.019}	0.255 _{0.022}	0.124 _{0.020}	0.736 _{0.0077}
	PCP	0.798 _{0.0028}	-0.197 _{0.030}	0.923 _{0.027}	0.719 _{0.038}	1.43 _{0.068}	0.642 _{0.0068}
	HD-PCP	0.799 _{0.0036}	-0.470 _{0.028}	0.713 _{0.019}	0.637 _{0.037}	0.936 _{0.083}	0.658 _{0.0081}
	C-PCP	0.802 _{0.0033}	-0.217 _{0.028}	2.63 _{1.4}	0.157 _{0.017}	0.0684 _{0.014}	0.758 _{0.0091}
	L-CP	0.801 _{0.0031}	0.0672 _{0.016}	24.9 _{2.1e+01}	0.106_{0.015}	0.0421_{0.0085}	0.782_{0.0082}
bio	M-CP	0.806 _{0.0028}	-1.07 _{0.023}	1.11 _{0.23}	0.113 _{0.012}	0.195 _{0.020}	0.760 _{0.0055}
	DR-CP	0.805 _{0.0029}	-1.40 _{0.022}	0.285_{0.0074}	0.517 _{0.040}	1.15 _{0.044}	0.642 _{0.0061}
	HDR-CP	0.807 _{0.0018}	-1.41_{0.024}	0.486 _{0.030}	0.0268 _{0.0058}	0.0198_{0.0046}	0.791 _{0.0056}
	PCP	0.805 _{0.0024}	-0.971 _{0.025}	6.76e+04 _{6.8e+04}	0.516 _{0.026}	1.20 _{0.028}	0.645 _{0.0063}
	HD-PCP	0.803 _{0.0027}	-1.27 _{0.023}	6.76e+04 _{6.8e+04}	0.320 _{0.016}	0.754 _{0.035}	0.677 _{0.0047}
	C-PCP	0.806 _{0.0028}	-1.06 _{0.030}	2.82 _{1.3}	0.0265_{0.0069}	0.0217 _{0.0065}	0.794_{0.0027}
	L-CP	0.802_{0.0027}	-1.23 _{0.024}	2.76 _{1.1}	0.0280 _{0.0052}	0.0203 _{0.0044}	0.786 _{0.0030}

Multi-Output Conformal Regression

Table 8: Full results obtained with the setup described in Section 6 (Part 4).

Dataset	Method	MC	G. Size	Size	CEC-X ($\times 100$)	CEC-Z ($\times 100$)	WSC
blog_data	M-CP	0.799 _{0.0031}	3.03e+15 _{3.0e+15}	∞	0.259 _{0.077}	0.127 _{0.056}	0.736 _{0.0084}
	DR-CP	0.806 _{0.0016}	-3.84_{0.35}	0.0760_{0.027}	1.20 _{0.15}	1.51 _{0.56}	0.635 _{0.014}
	HDR-CP	0.812 _{0.0028}	2.20e+15 _{2.2e+15}	∞	0.131 _{0.016}	0.0947 _{0.027}	0.774 _{0.0093}
	PCP	0.805 _{0.0030}	1.84e+18 _{1.8e+18}	∞	1.02 _{0.090}	1.55 _{0.48}	0.639 _{0.0072}
	HD-PCP	0.805 _{0.0036}	1.84e+18 _{1.8e+18}	∞	0.809 _{0.064}	0.989 _{0.29}	0.663 _{0.0081}
	C-PCP	0.806 _{0.0037}	1.84e+18 _{1.8e+18}	∞	0.0866_{0.028}	0.0808 _{0.021}	0.785_{0.0097}
	L-CP	0.800_{0.0016}	-2.87 _{0.28}	0.779 _{0.21}	0.199 _{0.074}	0.0773_{0.034}	0.748 _{0.013}
calcofi	M-CP	0.803 _{0.0028}	0.374 _{0.010}	2.08 _{0.019}	0.451 _{0.030}	0.463 _{0.028}	0.734 _{0.0079}
	DR-CP	0.802 _{0.0029}	0.197 _{0.0096}	1.48_{0.014}	1.45 _{0.046}	1.58 _{0.037}	0.648 _{0.0058}
	HDR-CP	0.805 _{0.0020}	0.0800_{0.0054}	1.98 _{0.018}	0.0213 _{0.0061}	0.0229 _{0.0054}	0.794 _{0.0033}
	PCP	0.800 _{0.0022}	0.570 _{0.0095}	2.28 _{0.022}	1.66 _{0.042}	1.81 _{0.036}	0.639 _{0.0050}
	HD-PCP	0.803 _{0.0026}	0.302 _{0.0095}	1.76 _{0.015}	0.962 _{0.027}	1.03 _{0.033}	0.685 _{0.0039}
	C-PCP	0.804 _{0.0024}	0.424 _{0.010}	2.91 _{0.020}	0.0183_{0.0055}	0.0197_{0.0069}	0.795_{0.0039}
	L-CP	0.800_{0.0022}	0.223 _{0.0076}	2.36 _{0.023}	0.0238 _{0.0057}	0.0220 _{0.0062}	0.788 _{0.0054}
taxi	M-CP	0.802 _{0.0027}	1.54 _{0.010}	5.86 _{0.068}	0.0707 _{0.0054}	0.0509 _{0.0039}	0.777 _{0.0036}
	DR-CP	0.803 _{0.0023}	0.983_{0.012}	2.73_{0.032}	0.428 _{0.017}	0.481 _{0.027}	0.704 _{0.0072}
	HDR-CP	0.811 _{0.0035}	1.04 _{0.016}	3.27 _{0.056}	0.0477 _{0.010}	0.0421 _{0.0073}	0.798 _{0.0050}
	PCP	0.803 _{0.0017}	1.45 _{0.011}	4.65 _{0.058}	0.367 _{0.014}	0.417 _{0.021}	0.711 _{0.0050}
	HD-PCP	0.804 _{0.0027}	1.20 _{0.015}	3.60 _{0.061}	0.199 _{0.015}	0.222 _{0.018}	0.739 _{0.0060}
	C-PCP	0.807 _{0.0024}	1.46 _{0.015}	5.31 _{0.083}	0.0266 _{0.0051}	0.0239 _{0.0036}	0.802_{0.0038}
	L-CP	0.802_{0.0034}	1.63 _{0.015}	6.63 _{0.079}	0.0257_{0.0032}	0.0185_{0.0037}	0.798 _{0.0039}

Supplementary Material for “Multi-Output Conformal Regression: A Unified Comparative Study with New Conformity Scores”

I Comparison between C-PCP and CP²-PCP

In this section, we compare our proposed method, C-PCP, introduced in the main paper, with the CP²-PCP method recently proposed by Plassier et al., 2024. More generally, we also compare the methods from the CP² framework of Plassier et al., 2024 with our class of CDF-based conformity scores (Section 3.1 in the main text). In Appendix I.1, we present the more general CP² framework using our own notation for clarity, with CP²-PCP as a particular case of CP². In Appendix I.2, we discuss the asymptotic properties of CP² and show the asymptotic equivalence with CDF-based methods. In Appendix I.3, we discuss the relationship between CDF-based and CP²-based methods.

I.1 The CP² method

Let us define a family of non-decreasing nested regions $\{\mathcal{R}(x; t)\}_{t \in \mathbb{R}}$ such that $\bigcap_{t \in \mathbb{R}} \mathcal{R}(x; t) = \emptyset$, $\bigcup_{t \in \mathbb{R}} \mathcal{R}(x; t) = \mathcal{Y}$, and $\bigcap_{t' > t} \mathcal{R}(x; t') = \mathcal{R}(x; t)$. Without loss of generality, these nested regions are expressed in terms of a conformity score $s_W(x, y) \in \mathbb{R}$ as follows:

$$\mathcal{R}(x; t) = \{y \in \mathcal{Y} : s_W(x, y) \leq t\}, \quad (91)$$

where $s_W(x, y)$ is continuous in y .

As the next step, we introduce a family of transformation functions $f_\tau(\lambda) : \mathbb{R} \rightarrow \mathbb{R}$ parameterized by $\tau \in \mathbb{R}$. It is assumed that for any τ , the function $\lambda \mapsto f_\tau(\lambda)$ is increasing and bijective. Let $\varphi \in \mathbb{R}$ be a constant (e.g. $\varphi = 1$). We also define the function $g_\varphi(\tau) = f_\tau(\varphi)$ and assume that $\tau \mapsto g_\varphi(\tau)$ is increasing and bijective.

As a first step towards defining CP², we construct a prediction region assuming knowledge of the conditional distribution $F_{Y|X}$. For a given input $x \in \mathcal{X}$, the prediction region is defined as:

$$\bar{R}_{\text{CP}^2}(x) = \mathcal{R}(x, f_{\tau_x}(\varphi)), \quad (92)$$

where

$$\tau_x = \inf \{\tau : \mathbb{P}(Y \in \mathcal{R}(X, f_\tau(\varphi)) \mid X = x) \geq 1 - \alpha\} \quad (93)$$

implies that $\bar{R}_{\text{CP}^2}(x)$ guarantees conditional coverage given x . Furthermore, using (91) and defining the random variable $W = s_W(X, Y)$, we can equivalently express (93) as

$$\tau_x = \inf \{\tau : \mathbb{P}(s_W(X, Y) \leq f_\tau(\varphi) \mid X = x) \geq 1 - \alpha\} \quad (94)$$

$$= \inf \{\tau : \mathbb{P}(g_\varphi^{-1}(s_W(X, Y)) \leq \tau \mid X = x) \geq 1 - \alpha\} \quad (95)$$

$$= Q_{g_\varphi^{-1}(W)}(1 - \alpha \mid X = x) \quad (96)$$

$$= g_\varphi^{-1}(Q_W(1 - \alpha \mid X = x)), \quad (97)$$

where we used that g_φ is increasing and bijective, with $g_\varphi^{-1}(f_\tau(\varphi)) = \tau$. In other words, τ_x is the $1 - \alpha$ quantile of $g_\varphi^{-1}(W)$.

However, in practice, τ_x cannot be computed directly since the true conditional distribution $F_{Y|x}$ is unknown. Instead, it can be estimated using a sample $\hat{Y}^{(k)}$, $k \in [K]$, drawn from the estimated conditional distribution $\hat{F}_{Y|x}$. If $\hat{Q}_W(1 - \alpha \mid X = x)$ is the $1 - \alpha$ quantile of the empirical distribution $\frac{1}{K} \sum_{k \in [K]} \delta_{s_W(x, \hat{Y}^{(k)})}$, we can compute

$$\hat{\tau}_x = g_\varphi^{-1}(\hat{Q}_W(1 - \alpha \mid X = x)). \quad (98)$$

It should be noted that this estimated prediction region loses the exact conditional and marginal coverage properties due to the reliance on the estimated conditional distribution. The following shows how conformal prediction can restore some coverage properties.

From (91), using (92), we can write

$$\bar{R}_{\text{CP}^2}(x) = \{y \in \mathcal{Y} : s_W(x, y) \leq f_{\tau_x}(\varphi)\} \quad (99)$$

$$= \{y \in \mathcal{Y} : f_{\tau_x}^{-1}(s_W(x, y)) \leq \varphi\}, \quad (100)$$

where we used the invertibility of f_τ for any $\tau \in \mathbb{R}$.

Inspired by (100), Plassier et al., 2024 defined the following conformity score:

$$s_{\text{CP}^2}(x, y) = f_{\hat{\tau}_x}^{-1}(s_W(x, y)), \quad (101)$$

for which the corresponding prediction region \hat{R}_{CP^2} is given by

$$\hat{R}_{\text{CP}^2}(x) = \{y \in \mathcal{Y} : s_{\text{CP}^2}(x, y) \leq \hat{q}\}, \quad (102)$$

where we used (2) from the main text.

As an example, taking $f_\tau(\lambda) = \tau\lambda$ and $\varphi = 1$, the conformity score becomes:

$$s_{\text{CP}^2}(x, y) = s_W(x, y)/\hat{\tau}_x, \quad (103)$$

where $\hat{\tau}_x$ is defined in (98). Finally, we obtain CP²-PCP simply by replacing s_W with s_{PCP} in (103).

I.2 Asymptotic properties

I.2.1 Asymptotic equivalence of prediction regions

In the following, we prove that the prediction regions generated by CP² (for any f_τ and φ) and CDF-based methods are identical in the oracle setting, asymptotically, as $|\mathcal{D}_{\text{cal}}| \rightarrow \infty$. Specifically, for any $x \in \mathcal{X}$, both methods select the same threshold $t_{1-\alpha} = Q_W(1 - \alpha \mid X = x)$ for the prediction region $\mathcal{R}(x; t_{1-\alpha})$, which ensures a coverage level of $1 - \alpha$.

Proposition 6. Provided that the assumptions in Appendix I.1 hold, for any $x \in \mathcal{X}$, the prediction regions $\bar{R}_{\text{CP}^2}(x)$ (for any choice of f_τ and φ) and $\bar{R}_{\text{CDF}}(x)$ are equivalent.

Proof. Using the fact that $g_\varphi^{-1}(f_\tau(\varphi)) = \tau$ for any $\tau \in \mathbb{R}$ and that g_φ is increasing and bijective, we can write:

$$\bar{R}_{\text{CP}^2}(x) = \{y \in \mathcal{Y} : s_W(x, y) \leq f_{\tau_x}(\varphi)\} \quad (104)$$

$$= \{y \in \mathcal{Y} : g_\varphi^{-1}(s_W(x, y)) \leq \tau_x\} \quad (105)$$

$$= \{y \in \mathcal{Y} : g_\varphi^{-1}(s_W(x, y)) \leq g_\varphi^{-1}(Q_W(1 - \alpha \mid X = x))\} \quad (106)$$

$$= \{y \in \mathcal{Y} : s_W(x, y) \leq Q_W(1 - \alpha \mid X = x)\}. \quad (107)$$

Let $\bar{R}_{\text{CDF}}(x)$ denote the prediction region obtained using the conformity score s_{CDF} as $|\mathcal{D}_{\text{cal}}| \rightarrow \infty$. As shown in Section 3.1, $s_{\text{CDF}}(X, Y) \sim \mathcal{U}(0, 1)$, which implies $\hat{q} = 1 - \alpha$. Therefore:

$$\bar{R}_{\text{CDF}}(x) = \{y \in \mathcal{Y} : s_{\text{CDF}}(x, y) \leq 1 - \alpha\} \quad (108)$$

$$= \{y \in \mathcal{Y} : F_{W|x}(s_W(x, y) \mid X = x) \leq 1 - \alpha\} \quad (109)$$

$$= \{y \in \mathcal{Y} : s_W(x, y) \leq Q_W(1 - \alpha \mid X = x)\}. \quad (110)$$

This shows that $\bar{R}_{\text{CP}^2}(x) = \bar{R}_{\text{CDF}}(x)$ and that the threshold $t_{1-\alpha} = Q_W(1 - \alpha \mid X = x)$ is identical for both methods.

□

I.2.2 Asymptotic conditional coverage

Proposition 7. Provided that the assumptions in Section 4.2 of the main text hold, specifically that $\hat{F}_{Y|x} = F_{Y|x}$ for all $x \in \mathcal{X}$, and $|\mathcal{D}_{\text{cal}}| \rightarrow \infty$, CP^2 achieves asymptotic conditional coverage as $K \rightarrow \infty$.

Proof. Under these assumptions, we have $\hat{Q}_W(\cdot | X = x) = Q_W(\cdot | X = x)$, which implies $\hat{\tau}_x = \tau_x$ for all $x \in \mathcal{X}$. Hence, the prediction region for CP^2 is given by:

$$\bar{R}_{\text{CP}^2}(x) = \{y \in \mathcal{Y} : s_{\text{CP}^2}(x, y) \leq \varphi\}.$$

Since this prediction region provides conditional coverage, it also ensures marginal coverage:

$$\mathbb{P}(Y \in \bar{R}_{\text{CP}^2}(X)) = \mathbb{P}(s_{\text{CP}^2}(X, Y) \leq \varphi) \quad (111)$$

$$= \mathbb{E}_X [\mathbb{P}(s_{\text{CP}^2}(X, Y) \leq \varphi | X)] \quad (112)$$

$$= \mathbb{E}_X [1 - \alpha] \quad (113)$$

$$= 1 - \alpha. \quad (114)$$

Since \hat{q} is the $1 - \alpha$ quantile of $s_{\text{CP}^2}(X, Y)$, and as $|\mathcal{D}_{\text{cal}}| \rightarrow \infty$, we have $\hat{q} = \varphi$ by definition. Therefore, since $\bar{R}_{\text{CP}^2}(x)$ achieves conditional coverage (see (93)), the region $\hat{R}_{\text{CP}^2}(x)$ also achieves asymptotic conditional coverage:

$$\mathbb{P}(Y \in \hat{R}_{\text{CP}^2}(X) | X = x) = \mathbb{P}(s_{\text{CP}^2}(X, Y) \leq \hat{q} | X = x) \quad (115)$$

$$= \mathbb{P}(s_{\text{CP}^2}(X, Y) \leq \varphi | X = x) \quad (116)$$

$$\geq 1 - \alpha. \quad (117)$$

□

I.3 Relationship between CDF-based and CP^2 -based methods

We observe that the difference between the conformity scores s_{ECDF} and s_{CP^2} with the same base conformity score s_W lies in the way they transform $s_W(x, y)$ to obtain asymptotic conditional coverage. Both methods rely on a sample $\{\hat{Y}^{(k)}\}_{k=1}^K$ where $\hat{Y}^{(k)} \sim \hat{F}_{Y|x}$.

Recall that the conformity scores s_{ECDF} and s_{CP^2} are given by

$$s_{\text{ECDF}}(x, y) = \frac{1}{K} \sum_{k \in [K]} \mathbb{I}(s_W(x, \hat{Y}^{(k)}) \leq s_W(x, y)) = \hat{F}_{W|x}(s_W(x, y)), \quad (118)$$

$$s_{\text{CP}^2}(x, y) = f_{\hat{\tau}_x}^{-1}(s_W(x, y)) \text{ where } \hat{\tau}_x = g_{\varphi}^{-1}(\hat{Q}_W(1 - \alpha | X = x)). \quad (119)$$

A natural question is whether there exists f_{τ} and φ (with the assumptions introduced in Appendix I.1) such that these two methods produce the same regions. Given $x \in \mathcal{X}$, when K is finite, we observe that the conformity score $s_{\text{ECDF}}(x, \cdot)$ is discontinuous and is thus necessarily different from the conformity score $s_{\text{CP}^2}(x, \cdot)$, which is continuous.

Thus, we turn our attention to a setting where $K \rightarrow \infty$ and $s_{\text{ECDF}}(x, \cdot)$ becomes continuous. In Proposition 8, we show that, in the particular case where the conditional distributions $\{\hat{F}_{W|x}\}_{x \in \mathcal{X}}$ belong to a location family, there exists an f_{τ} and φ such that the two methods are equivalent.

However, the proof is not easily generalizable to a location-scale family. Further development of existing classes of conformal methods with asymptotic conditional coverage and their intersections is a promising avenue for research. Future work could also focus on identifying scenarios where a particular conformity score minimizes region sizes while still achieving asymptotic conditional coverage.

Proposition 8. Consider a scenario where all conditional distributions $\{\hat{F}_{W|x}\}_{x \in \mathcal{X}}$ belong to a location family, i.e.,

$$\hat{F}_{W|x}(w) = F(w - \hat{\mu}_x) \text{ and } \hat{Q}_{W|x}(\alpha) = F^{-1}(\alpha) + \hat{\mu}_x, \quad (120)$$

for some continuous and strictly increasing base CDF F and location parameter $\hat{\mu}_x$. The conformity scores s_{ECDF} and s_{CP^2} lead to the same prediction regions as $K \rightarrow \infty$.

Proof. We will show that there is a transformation function f_τ with the assumptions above such that, for any $x \in \mathcal{X}$ and $w \in \mathbb{R}$,

$$f_{\hat{\tau}_x}^{-1}(w) = \hat{F}_{W|x}(w \mid X = x) \quad (121)$$

$$\text{where } \hat{\tau}_x = g_\varphi^{-1}(\hat{Q}_{W|x}(1 - \alpha \mid X = x)). \quad (122)$$

Define the transformation function f_τ as:

$$f_\tau(\lambda) = F^{-1}(\lambda) + \tau, \quad (123)$$

where $\tau > 0$, and define $\varphi = 1 - \alpha$.

The inverse transformations are:

$$f_\tau^{-1}(\lambda) = F(\lambda - \tau), \quad (124)$$

and

$$g_\varphi^{-1}(w) = w - F^{-1}(\varphi). \quad (125)$$

Now, compute

$$\hat{\tau}_x = F^{-1}(1 - \alpha) + \hat{\mu}_x - F^{-1}(\varphi) = \hat{\mu}_x. \quad (126)$$

Finally, we obtain

$$f_{\hat{\tau}_x}^{-1}(w) = F(w - \hat{\tau}_x) = F(w - \hat{\mu}_x) = \hat{F}_{W|x}(w). \quad (127)$$

□

J Relationship between conformity scores and regions

Section 2.2 and Section 3 in the main text presented several multi-output conformal methods through their conformity score s . As explained in Section 2.1, their corresponding prediction region \hat{R} can be computed as follows:

$$\hat{R}(x) = \{y \in \mathcal{Y} : s(x, y) \leq \hat{q}\}.$$

In this section, we explicitly derive the prediction region associated with these methods.

M-CP. Following Zhou et al., 2024b, we show that the prediction region $\hat{R}_{\text{M-CP}}$ can be derived from $s_{\text{M-CP}}$ as follows:

$$s_{\text{M-CP}}(x, y) \leq \hat{q} \iff \max_{i \in [d]} s_i(x, y_i) \leq \hat{q} \quad (128)$$

$$\iff \forall i \in [d], s_i(x, y_i) \leq \hat{q} \quad (129)$$

$$\iff \forall i \in [d], \max\{\hat{l}_i(x) - y_i, y_i - \hat{u}_i(x)\} \leq \hat{q} \quad (130)$$

$$\iff \forall i \in [d], \hat{l}_i(x) - y_i \leq \hat{q} \wedge y_i - \hat{u}_i(x) \leq \hat{q} \quad (131)$$

$$\iff \forall i \in [d], \hat{l}_i(x) - \hat{q} \leq y_i \wedge y_i \leq \hat{u}_i(x) + \hat{q} \quad (132)$$

$$\iff \forall i \in [d], y_i \in [\hat{l}_i(x) - \hat{q}, \hat{u}_i(x) + \hat{q}] \quad (133)$$

$$\iff y_i \in \bigtimes_{i=1}^d [\hat{l}_i(x) - \hat{q}, \hat{u}_i(x) + \hat{q}] \quad (134)$$

$$\iff y \in \hat{R}_{\text{M-CP}}(x). \quad (135)$$

DR-CP The equivalence is straightforward.

HDR-CP. Given $\hat{Y} \sim \hat{f}(\cdot | X = x)$ and $U = \hat{f}(\hat{Y} | X = x)$, for any $y \in \mathcal{Y}$, we can write

$$s_{\text{HDR-CP}}(x, y) \tag{136}$$

$$= \text{HPD}_{\hat{f}}(y | x) \tag{137}$$

$$= \mathbb{P}(\hat{f}(\hat{Y} | x) \geq \hat{f}(y | x) | X = x) \tag{138}$$

$$= \mathbb{P}(U \geq \hat{f}(y | x) | X = x) \tag{139}$$

$$= 1 - \mathbb{P}(U \leq \hat{f}(y | x) | X = x) \tag{140}$$

$$= 1 - F_U(\hat{f}(y | x) | X = x), \tag{141}$$

where $F_U(\cdot | X = x)$ is the conditional CDF of U given $X = x$.

Recall that the prediction region for **HDR-CP** is given by

$$\hat{R}_{\text{HDR-CP}}(x) = \{y \in \mathcal{Y} : \hat{f}(y | x) \geq t_{\hat{q}}\}, \quad \text{where } t_{\hat{q}} = \sup\{t : \mathbb{P}(\hat{f}(\hat{Y} | x) \geq t | X = x) \geq \hat{q}\}. \tag{142}$$

The threshold $t_{\hat{q}}$ in (142) can be equivalently written as follows:

$$t_{\hat{q}} = \sup\{t : \mathbb{P}(\hat{f}(\hat{Y} | x) \geq t | X = x) \geq \hat{q}\} \tag{143}$$

$$= \sup\{t : \mathbb{P}(U \geq t | X = x) \geq \hat{q}\} \tag{144}$$

$$= \sup\{t : 1 - \mathbb{P}(U \leq t | X = x) \geq \hat{q}\} \tag{145}$$

$$= \sup\{t : 1 - \hat{q} \geq F_U(t | X = x)\} \tag{146}$$

$$= F_U^{-1}(1 - \hat{q} | X = x), \tag{147}$$

where we use the definition of the upper quantile function in the last step.

Using (136), (142), and (147), we can write

$$s_{\text{HDR-CP}}(x, y) \leq \hat{q} \iff \text{HPD}_{\hat{f}}(y | x) \leq \hat{q} \tag{148}$$

$$\iff 1 - F_U(\hat{f}(y | x) | X = x) \leq \hat{q} \tag{149}$$

$$\iff F_U(\hat{f}(y | x) | X = x) \geq 1 - \hat{q} \tag{150}$$

$$\iff \hat{f}(y | x) \geq F_U^{-1}(1 - \hat{q} | X = x) \tag{151}$$

$$\iff \hat{f}(y | x) \geq t_{\hat{q}} \tag{152}$$

$$\iff y \in \hat{R}_{\text{HDR-CP}}(x). \tag{153}$$

PCP. Let $B(\mu, r)$ represent a ball with center μ and radius r . Following Wang et al., 2023b, we show that, for any $x \in \mathcal{X}$, $\hat{R}_{\text{PCP}}(x)$ corresponds to a union of balls:

$$s_{\text{PCP}}(x, y) \leq \hat{q} \iff \min_{l \in [L]} \|y - \tilde{Y}^{(l)}\|_2 \leq \hat{q} \tag{154}$$

$$\iff \exists l \in [L], \|y - \tilde{Y}^{(l)}\|_2 \leq \hat{q} \tag{155}$$

$$\iff \exists l \in [L], y \in B(\tilde{Y}^{(l)}, \hat{q}) \tag{156}$$

$$\iff y \in \bigcup_{l \in [L]} B(\tilde{Y}^{(l)}, \hat{q}) \tag{157}$$

$$\iff y \in \hat{R}_{\text{PCP}}(x), \tag{158}$$

where $\tilde{Y}^{(l)} \sim \hat{F}_{Y|x}, l \in [L]$.

HD-PCP. For **HD-PCP**, the reasoning is similar to **PCP** with the difference that only the $\lfloor (1 - \alpha)L \rfloor$ samples with the highest density are kept.

CDF-based conformity scores. We note that the region $\hat{R}_{\text{CDF}}(x)$ has a similar form to $\hat{R}_W(x) = \{y \in \mathcal{Y} : s_W(x, y) \leq \hat{q}\}$, except that the threshold on $s_W(x, y)$ is different and depends on x . In fact, we can write

$$\hat{R}_{\text{CDF}}(x) = \{y \in \mathcal{Y} : s_{\text{CDF}}(x, y) \leq \hat{q}\} \quad (159)$$

$$= \{y \in \mathcal{Y} : F_{W|X=x}(s_W(x, y) | X = x) \leq \hat{q}\} \quad (160)$$

$$= \{y \in \mathcal{Y} : s_W(x, y) \leq F_{W|X=x}^{-1}(\hat{q} | X = x)\}. \quad (161)$$

In the special case where $s_W = s_{\text{PCP}}$, since PCP always generates predictions as a union of balls, we can conclude that C-PCP will do the same.

Latent-based conformity scores. Since $\hat{Q}(\cdot; x)$ is bijective, for every $y \in \mathcal{Y}$, there exists a unique $z \in \mathcal{Z}$ such that $y = \hat{Q}(z; x)$. Therefore, the condition $d_{\mathcal{Z}}(\hat{Q}^{-1}(y; x)) \leq \hat{q}$ is equivalent to $d_{\mathcal{Z}}(z) \leq \hat{q}$, where $z = \hat{Q}^{-1}(y; x)$. This gives us the prediction region:

$$\hat{R}_{\text{L-CP}}(x) = \{y \in \mathcal{Y} : d_{\mathcal{Z}}(\hat{Q}^{-1}(y; x)) \leq \hat{q}\} \quad (162)$$

$$= \{\hat{Q}(z; x) : z \in \mathcal{Z} \text{ and } d_{\mathcal{Z}}(z) \leq \hat{q}\}. \quad (163)$$

K Estimator for the region size

In this section, we discuss the efficiency of the region size estimator introduced in Appendix A.3. This estimator is based on a density estimator $\hat{f}(\cdot | x)$ and a sample $\hat{Y}^{(k)}, k \in [K]$, drawn i.i.d. from the conditional distribution $Y | X = x$ for any $x \in \mathcal{X}$. Specifically, the estimator is given by:

$$\hat{V}(x) = \frac{1}{K} \sum_{k=1}^K \frac{\mathbb{1}(\hat{Y}^{(k)} \in \hat{R}(x))}{\hat{f}(\hat{Y}^{(k)} | x)}.$$

While the estimator is unbiased, i.e., $\mathbb{E}[\hat{V}(x)] = |\hat{R}(x)|$, we want to study its variance. Let $I = \mathbb{1}(\hat{Y} \in \hat{R}(x))$ represent the indicator that a sample \hat{Y} lies within the prediction region $\hat{R}(x)$, and let $\rho = \mathbb{P}(\hat{Y} \in \hat{R}(x))$ denote the coverage probability obtained from the samples based on our density estimator. Using the law of total variance, we obtain the following expression for the variance of $\hat{V}(x)$:

$$\begin{aligned} \mathbb{V}[\hat{V}(x)] &= \frac{1}{K} \mathbb{V}\left[\frac{I}{\hat{f}(\hat{Y} | x)}\right] \\ &= \frac{1}{K} \left(\mathbb{E}\left[\mathbb{V}\left[\frac{I}{\hat{f}(\hat{Y} | x)} \mid I\right]\right] + \mathbb{V}\left[\mathbb{E}\left[\frac{I}{\hat{f}(\hat{Y} | x)} \mid I\right]\right] \right) \\ &= \frac{1}{K} \left(\rho \mathbb{V}\left[\frac{1}{\hat{f}(\hat{Y} | x)}\right] + \rho(1 - \rho) \mathbb{E}\left[\frac{1}{\hat{f}(\hat{Y} | x)}\right]^2 \right). \end{aligned}$$

Assuming that the density estimate corresponds to the true density, i.e. $\hat{f}(\cdot | x) = f_{Y|x}(\cdot | x)$ and that \hat{R} achieves conditional coverage, then $\rho = 1 - \alpha$, and we obtain:

$$\mathbb{V}[\hat{V}(x)] = \frac{1}{K} \left((1 - \alpha) \mathbb{V}\left[\frac{1}{f_{Y|x}(Y | x)}\right] + \alpha(1 - \alpha) \mathbb{E}\left[\frac{1}{f_{Y|x}(Y | x)}\right]^2 \right).$$

This indicates that the variance of our estimator only depends on the variance and expectation of the random variable $\frac{1}{f(Y|x)}$. In this case, the variance does not directly depend on the output dimension d .

Figure 10 shows how the estimator behaves in a scenario with a specific density estimator and prediction region with varying output dimension d and an 80% coverage level. Since there is no dependence on X , we abbreviate the notation as follows: $\hat{R} = \hat{R}(x)$, $\hat{f}(y) = \hat{f}(y | x)$, and $\hat{V} = \hat{V}(x)$ for any $x \in \mathcal{X}$. The density estimator is a standard

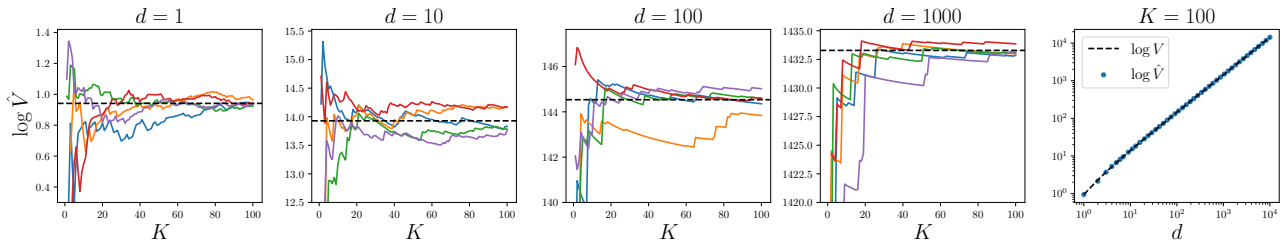


Figure 10: Panels 1 to 4: Trajectories of the log volume estimator with increasing K compared to the true log volume (dashed line) for different output dimensions d . Panel 5: Log volume estimator with $K = 100$ compared to the true log volume (dashed line).

normal distribution $\hat{f}(y) = \mathcal{N}(y; 0, I_d)$ and the prediction region is a ball $\hat{R} = \{y \in \mathcal{Y} : \|y\|_2 \leq F_{\chi_d^2}^{-1}(1 - \alpha)\}$, where χ_d^2 is the chi-squared distribution with d degrees of freedom and $F_{\chi_d^2}^{-1}$ is its quantile function. It can be shown that $\mathbb{P}_{\hat{Y} \sim \hat{f}(\cdot)}(\hat{Y} \in \hat{R}) = 1 - \alpha$. In this case, the volume V of \hat{R} can be computed exactly.

Each of the first four panels in Figure 10 shows five trajectories for $\log \hat{V}$ as K increases from 1 to 100. The true volume, $\log V$, of the prediction region is indicated by a dashed line. We observe that the estimator converges within a reasonable range of the true volume for varying output dimensions d . The last panel illustrates the value of $\log \hat{V}$ as a function of d , with $\log V$ again marked by a dashed line. From this, we observe that the estimator remains close to the true volume across different output dimensions d .

L Further related studies

Beyond the references cited in the main text, our research builds on a broad body of literature that spans several closely related themes. This supplementary section provides a concise overview of these topics.

In the realm of multivariate functional data, Diquigiovanni et al., 2022 introduced conformal predictors that create adaptive, finite-sample valid prediction bands, with extensions into time series applications, particularly in energy markets (Diquigiovanni et al., 2021).

For multi-step-ahead or multi-horizon forecasting, predictions can be made across multiple outputs simultaneously rather than sequentially, aligning with a multi-output forecasting framework. Stankeviciute et al., 2021 explored multi-horizon time series forecasting using recurrent neural networks (RNNs), incorporating univariate conformal techniques with nominal coverage adjustments via Bonferroni correction. Similarly, English et al., 2024 adapted the Amplitude-Modulated L-inf norm method from Diquigiovanni et al., 2023 for multi-output, multi-step forecasting.

In multi-target regression, Messoudi et al., 2021 applied copula functions in deep neural networks to provide multivariate predictions with guaranteed coverage. Their findings suggest that simple parametric copulas can work for certain datasets, but more complex copulas may be required for well-calibrated predictions, which introduces challenges, as complex copulas typically require significant calibration data. Building on this, Sun and Yu, 2022 proposed a copula-based method for multi-step time series forecasting, optimizing the calibration and efficiency of confidence intervals. However, this method requires two calibration phases and is primarily feasible with large calibration datasets. Moreover, its validity relies on the empirical copula, limiting applicability to other learnable copula classes. One very recent advancement on the subject, following ideas expressed by Messoudi et al., 2021 in their conclusions, is Park et al., 2024, where the dependence structure between marginal distributions is recovered via the use of vine copulas.

Another set of methodologies that tackle multi-output problems are based on multiplicity-correction approaches for multiple testing. Timans et al., 2024 uses permutation tests, and obtains a globally valid prediction.

In the context of conformal prediction, the flexibility in configuring the prediction region is a degree of freedom for the modeler. To overcome the limitations of traditional hyper-rectangular prediction regions, Messoudi, 2022 introduced ellipsoidal uncertainty sets that enable instance-specific adaptation of confidence regions. Johnstone and Ndiaye, 2022 advanced multi-output regression by developing efficient techniques for approximating conformal

prediction sets without retraining the model, although their approach relies heavily on the predictive model being a linear function of Y . Xu et al., 2024 constructed ellipsoidal prediction regions for time series, capable of modeling dependencies between outputs, though this method does not handle multimodality. Our work closely connects with the multivariate conformal prediction literature, where multi-horizon prediction is viewed as a prediction across multiple outputs.

Overall, as this study demonstrates, the flexibility of conformal prediction allows for coherent handling of diverse data types. Multi-output problems represent one facet of a broader taxonomy, as explored by Zhou et al., 2024a, who discuss further developments in multi-output conformal prediction.